Modeling fluid transfer along California faults when integrating pressure solution crack sealing and compaction processes

Jean-Pierre Gratier, Pascal Favreau, and François Renard

Laboratoire de Géophysique Interne et Tectonophysique, CNRS Observatoire, Université Joseph Fourier, Geosciences, Grenoble, France

Received 12 July 2000; revised 7 March 2002; accepted 26 April 2002; published 19 February 2003.

[1] Several models pertaining to earthquake cycles imply intermittent fluid flow through fault. During the interseismic period, increase in fluid pressure from hydrostatic to lithostatic values is a crucial parameter in mechanisms leading to earthquakes. To achieve such pressures, geodynamic processes (gouge compaction, fluid flow) and changes in permeability are required. Previous models have postulated that changes in permeability (by self-healing) are faster than the effects of geodynamic processes. We consider the different mechanisms and rates of crack sealing near active fault on the examples of uplifted Californian faults. We find that natural crack sealing is normally not achieved by a rapid self-healing process. Pressure solution, with mass transfer from solution cleavage to cracks, appears to be a more important mechanism for crack sealing and creep during postseismic deformation. The geometry of transfer path and experimental data have been used to model crack sealing rates by pressure solution which are estimated to be rather slow, similar to the recurrence time of some earthquakes. Such slow changes in permeability may be crucial factors in controlling the increase in fluid pressure and, consequently, the mechanism of critical failure in faults. Then, numerical modeling of fluid pressure and transfer around active faults has been performed integrating a slow change in permeability by crack sealing, gouge compaction, and fluid flow from depth. This modeling shows various location and evolution of fluid overpressure during the interseismic period depending on these processes and allows one to estimate the amount of fluid transferred from depth during interseismic periods. *INDEX TERMS:* 8010 Structural Geology: Fractures and faults; 7209 Seismology: Earthquake dynamics and mechanics; 8045 Structural Geology: Role of fluids; 8159 Tectonophysics: Evolution of the Earth: Rheology—crust and lithosphere; 5139 Physical Properties of Rocks: Transport properties; *KEYWORDS:* fault, creep, transfer, fluid, sealing, dissolution

Citation: Gratier, J.-P., P. Favreau, and F. Renard, Modeling fluid transfer along California faults when integrating pressure solution crack sealing and compaction processes, *J. Geophys. Res.*, *108*(B2), 2104, doi:10.1029/2001JB000380, 2003.

1. Introduction

[2] To account for the low frictional heating and the lack of strength of active faults, as inferred from low heat flow measurements [*Lachenbruch*, 1980], and in situ stress orientations [*Hickman and Evans*, 1991], earthquakes are postulated to occur when fluid pressures are close to lithostatic levels. However, because of dilatancy and fault network connection, earthquakes are also thought to induce permeability change in the country rock and can therefore temporarily reduce fluid pressures to hydrostatic values [*Sibson*, 1992b; *Chester et al.*, 1993; *Boullier and Robert*, 1992]. Consequently, because of progressive weakening of the fault, fluid pressure in fault zones is expected to change from near hydrostatic value after an earthquake to near lithostatic value before the next earthquake.

0148-0227/03/2001JB000380$09.00

[3] Evidence for high fluid pressures has been found in tectonically active areas. On the basis of borehole records from gas and oil wells, *Hubbert and Rubey* [1959] and *Berry* [1973] showed many examples of pore pressures largely above hydrostatic pressures, sometimes even approaching lithostatic pressures at depths ranging from 0.3 to 4 km. At greater depth (from 6 to 10 km) in the Alps, comparisons between fluid density in horizontal veins (from fluid inclusion studies), temperature (from K/Na ratios), and the thickness of the cover, showed that fluid pressures in these veins were very close to lithostatic values [*Poty et al.*, 1974; *Bernard et al.*, 1977]. In parallel, evidence of hydrostatic fluid pressure has also been found, in boreholes, associated with critically stressed faults in the crust [*Zoback*, 1999]. This leads to the ideas that fluid pressure temporarily varies in fault zones [*Robert et al.*, 1995] and that fault networks and associated crack sealing play a critical role in controlling permeability and fluid pressure at depth [*Scholz*, 1990].

[4] To achieve high fluid pressures in seismic zones, different geodynamic processes have been proposed, such

as flow of fluids from depth at high pressure [*Sibson*, 1977; *Byerlee*, 1990; *Rice*, 1992], and compaction within fault gouges [*Sleep and Blanpied*, 1992]. In these models, rapid sealing of cracks, leading to a fast decrease in permeability, is postulated to occur in the country rock after the occurrence of an earthquake. Consequently, the subsequent increase in fluid pressure is assumed to be only dependent on the rates of geodynamic processes. This assumption of rapid sealing is based upon experimental results of crack healing [*Smith and Evans*, 1984; *Wilkins et al.*, 1985; *Brantley et al.*, 1990]. Crack healing is driven by the lowering of crack-free surface energy. This occurs without any input of matter in the crack. However, such a healing process may not necessarily be the dominant mechanism associated with natural change in permeability. Crack healing occurs mainly at grain scale. For larger cracks and fractures the only way to achieve closure is through sealing. It will be shown in this paper that processes of crack sealing, which imply input of matter in the crack and which are much slower than crack healing, are found near active faults. Estimating the mechanism and the kinetics of crack sealing around active faults is thus a crucial goal since the kinetics of sealing controls the rate of change of permeability in the country rock. If the kinetics of crack sealing is not fast relative to the rates of the geodynamic processes, crack sealing processes may be a key factor in controlling the rate of increase in fluid pressure during the interseismic period. Consequently, the rate of change of permeability may also play a key role in the mechanisms associated with critical fault failure. For example, it has been shown recently that the controlling parameter of the fluid-controlled earthquake may be the ratio of pore pressure increase versus shear stress accumulation [*Miller et al.*, 1996, 1999].

[5] In this paper, the various driving forces for crack sealing are first discussed. This emphasizes the key observations used to discriminate between the various mechanisms of crack sealing. The parameters required to estimate the kinetics of crack sealing processes are then discussed. Finally, numerical modeling of fluid pressure and transfer through active faults is presented and discussed with reference to the example of Californian faults.

2. Crack Sealing Mechanisms and Kinetics

2.1. Various Mechanisms of Crack Sealing

[6] Mechanical compression can lead to crack closure [*Brace*, 1972]. Nonetheless, as cracks often open perpendicular to the direction of least effective stress, their closure after an earthquake implies that the effective stress magnitude varies, either by a decrease in the fluid pressure, or by a change in the state of stress. However, if the decrease in permeability is only linked to mechanical closure, the progressive increase in fluid pressure should easily re-open the closed cracks.

[7] Chemical effects leading to change in fluid solubility are more efficient for producing crack sealing by irreversible mass transfer. Temperature changes can lead to the sealing of large fractures, based on a change in mineral solubility. However, this effect is not the same for all minerals. For example, quartz and calcite display regular and inverse solubility versus temperature dependencies, respectively [*Fyfe et al.*, 1978]. For the case of a normal solubility-temperature dependence, a progressive decrease in temperature leads to widespread precipitation [*Cathles*, 1977]. Fluid pressure changes generally have only a small effect on mineral solubility. An exception to this is the case of fluid boiling [*Hedenquist et al.*, 1992], which may be induced by a pressure drop associated with earthquakes [*Sibson*, 1987]. Boiling results in the partitioning of aqueous constituents between a vapor and an aqueous phase; the heat of vaporization lost by the fluid results in a drop in temperature, potentially resulting in precipitation reactions at the low fluid pressure required for fluid boiling. Fluid composition and pH changes can also lead to either precipitation (fluid supersaturation) or dissolution (fluid undersaturation) in open veins [*Brimhall and Crerar*, 1987]. With all these effects, crack sealing is associated with infiltration of fluids into the matrix with two consequences:

1. When considering the irregular nature of paths associated with fluid flow, only the narrowest passages are sealed by fluid infiltration. Complete sealing is difficult since, after the sealing of the narrowest paths, isolated void spaces still remain open. Euhedral crystals grow in such open voids.

2. The solubility of minerals in solution is never very high, for example: 0.1 wt% of quartz in solution at 300°C [*Kennedy*, 1950]. Consequently, even in the case of a drastic decrease in temperature, the ratio between aqueous fluid and mineral deposit is high (3×10^4) implicating huge quantities of water percolating through the rocks to seal the cracks. Special conditions would therefore be required to produce systematic and complete crack sealing by these effects.

[8] Surface energy lowering and stress induced chemical reactions are alternative driving forces for mass transfer which can lead to the destruction of crack porosity via crack sealing. Different mechanisms may be operative, depending on the aperture of the cracks [*Wilkins et al.*, 1985] (Figure 1).

1. For the case of small aperture cracks (0.3–3 μm) (Figure 1a), crack healing is driven by a lowering of the crack-free surface energy [*Smith and Evans*, 1984; *Wilkins et al.*, 1985; *Brantley et al.*, 1990], and is the result of mass redistribution within an individual crack. Solid-to-solid contacts are needed along the fracture (Figure 1a, bottom, enlargement) in order to establish some bridges between the two walls of the fracture. Mass transfer occurs from the highest surface energy sites (large curvature surface) toward the lowest ones (low curvature sites near the solid/solid contacts) [*Kingery et al.*, 1976]. This mechanism may be evidenced by trails of fluid inclusions along the healed crack surfaces (Figure 1a, top) which represent the minimum of the surface energy after crack healing [*Gratier and Jenatton*, 1984; *Boullier et al.*, 1989].

2. The sealing of large aperture cracks (10 μm to millimeters to centimeters) (Figure 1b), with large opening of the walls of the fracture and without any contact between the walls, needs an influx of material into the cracks from outside sources. Such sources may be associated with pressure solution. This is commonly found in naturally occurring crack seal structures [*Ramsay*, 1980; *Groshong*, 1988; *Gratier and Gamond*, 1990]. This mechanism may be recognized directly by optical microscope, by chemical analysis or by cathodoluminescence studies. Mass transfer is proportional to the difference in chemical potential

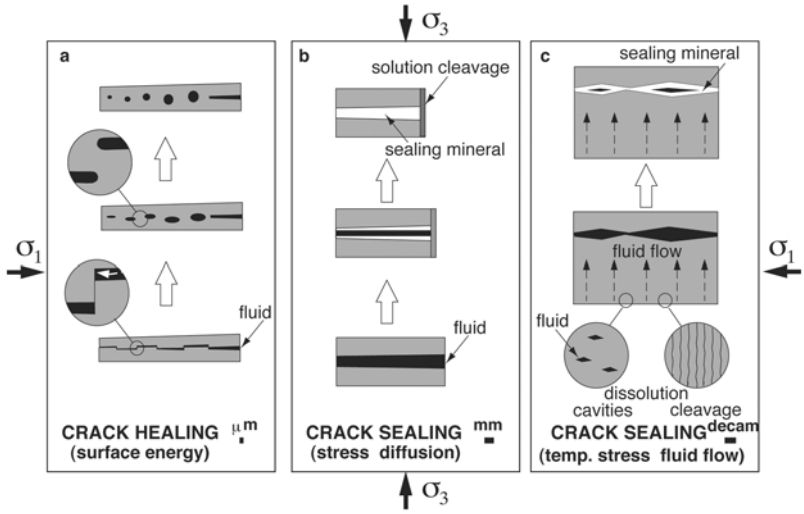

Figure 1. Various mechanisms of crack sealing from microcrack healing to regional crack sealing. Time-dependent change is from the bottom to the top (open arrows). (a) Crack healing driven by the lowering of microcrack surface energy. No input of external material, mass transfer occurs in free fluid (black) from site with maximum curvature to site with minimum curvature (white arrow), and trails of fluid inclusions mark the healed seams. (b) Crack sealing driven by differential stress with diffusion through the trapped fluid. Mass transfer occurs from solution cleavage to fracture with complete sealing of the veins. (c) Crack sealing with fluid flow. The sealing process may involve various driving forces (including temperature and stress), euhedral crystals grow in open cavities, and mass transfer occurs either from open cavities (free fluid) or from stress-driven solution cleavage (trapped fluid).

between the dissolution zone and the deposition zone. Various driving forces can lead to such chemical potential gradients which are either controlled by the difference in normal stress between solid/fluid interfaces or the difference in strain energy (elastic or plastic stored energy) [*Paterson*, 1973]. Most often, soluble species are removed from grain-to-grain contacts (stylolites or solution cleavage) and reprecipitated in veins or voids [*Weyl*, 1959; *Arthaud and Mattauer*, 1969; *Rutter*, 1983; *Gratier*, 1987]. In this case, mass transfer occurs by diffusion through the fluid phase trapped in the stressed contact. This mechanism can lead to the complete sealing of veins and voids (Figure 1b, top).

3. Moreover, on the basis of the evidence of large volume change on a regional scale, evidence of fluid infiltration coupled with diffusion has also been reported (Figure 1c) [*Etheridge et al.*, 1984; *McCaig and Knipe*, 1990; *Gratier and Gamond*, 1990; *Marquer and Burkhard*, 1992].

2.2. Kinetics of Solution-Deposition Transfer

[9] Regardless of the driving forces of the chemical processes and the mass transfer process in the upper crust solution, transfer processes require three sequential steps. The first step is the dissolution into a fluid phase in the zone with the highest chemical potential, the second is the mass transfer by diffusion (coupled or not with infiltration), the last is the precipitation at the fluid/mineral interface with the lowest chemical potential [*Raj*, 1982]. If one of these three ''in series'' sequential processes is much slower that the others, it will determine the overall sealing rate [*Fisher and Brantley*, 1992]. In rocks subjected to nonhydrostatic stresses, mass transfer may occur via two different types of fluid phases either free fluid or trapped fluid.

1. Mass transfer between dissolution and deposition sites may occur exclusively via an intergranular free fluid phase, as pointed out by various authors [*Bathurst*, 1987; *Engelder*, 1982; *Wintsch and Dunning*, 1985; *Tada and Siever*, 1986; *Gratier*, 1993]. In this case the driving forces of mass transfer may be the effect of free surface energy (linked to the difference in surface curvature), and the effect of dislocation strain and elastic strain changes along free mineral surfaces. This may also include the effect of pressure, temperature, and fluid composition as driving forces when the entire mass transfer path comprises a free fluid phase. When mass transfer occurs via such a free fluid, diffusion coefficients are high, for example, 10^{-8} m^2 s^{-1} for silica at 350°C [*Ildefonse*, 1980]. In such case, the limiting process is often the rate of mass exchange between solid and solution (dissolution or deposition rate). This is the case, for example, for the change in shape of small cavities in quartz at 350°C, driven by the difference in surface curvature [*Gratier and Jenatton*, 1984]. This is also the case of crack healing which is the same process as the change in shape of fluid inclusion [*Smith and Evans*, 1984; *Wilkins et al.*, 1985].

2. Mass transfer between dissolution and deposition sites may also occur at least partially along fluid phases trapped within loaded solid faces either as continuous fluid films [*Weyl*, 1959; *Rutter*, 1983], or as networks of fluid inclusions [*Raj and Chyung*, 1981; *Gratz*, 1991; *Spiers and Brzesowsky*, 1993]. This is the case when dissolution occurs along grain-to-grain contacts, stylolites and solution cleavage surfaces [*Groshong*, 1988]. Given the small thickness of this fluid phase and the slow diffusivity along it, mass transfer flux by diffusion through the trapped fluid is much slower than in a free fluid. From pressure solution

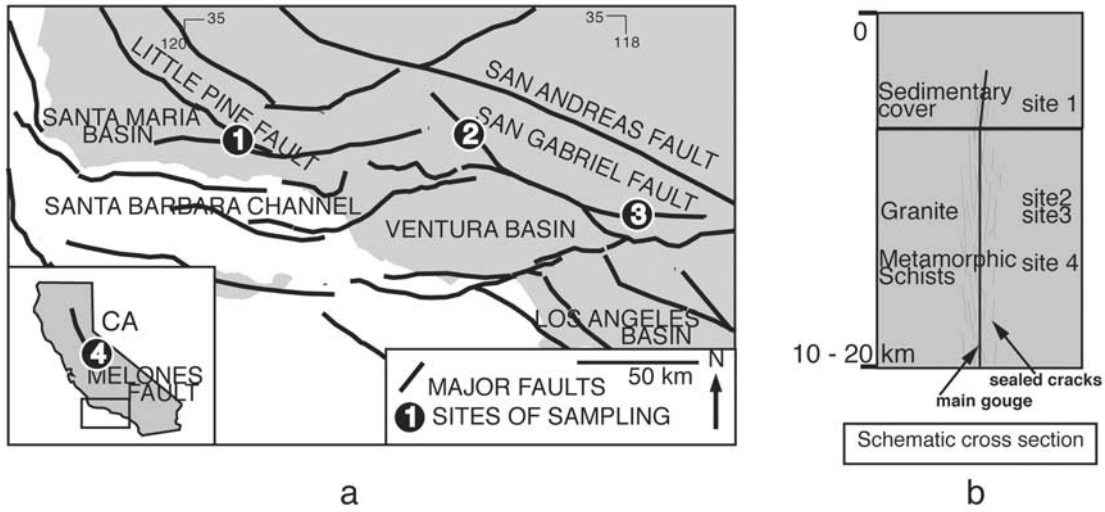

Figure 2. (a) Schematic map indicating the locations of the sampling sites: site 1, Little Pine fault; sites 2 and 3, San Gabriel fault; site 4, Melones fault (Mother Lode valley). Fault map of the Transverse Ranges Province adapted from *Jennings* [1994]. (b) Schematic cross section of a synthetic California strike slip fault affecting the entire seismic crust, with indication of the level of the various sampling sites.

experiments this flux (product diffusion times thickness) ranges from 10^{-19} to 10^{-21} m^3 s^{-1} for water film diffusion at 350°C (data taken from *Gratier and Guiguet* [1986] and *Rutter* [1976], respectively). In this case the overall process is mostly diffusion limited, the displacement rate of the dissolution interface being inversely proportional to the area of diffusion through the trapped fluid. The size of the elementary mean area of diffusion through the trapped fluid is related either to the grain size of the aggregates [*Elliot*, 1976; *Rutter*, 1976] or to the spacing of a network of microcracks [*Gratz*, 1991; *den Brok*, 1998; *Gratier et al.*, 1999b]. However, diffusion is not always the limiting process. For example, for quartz at low temperature, the kinetics of reaction is so slow that it may become the limiting process [*Oelkers et al.*, 1996]. The main difference between reaction rate and diffusion rate limited pressure solution laws is the difference in the dependence on the geometry of the mass transfer path [*Raj*, 1982]. A transitional pressure solution model integrating all the various limiting processes has been developed by *Renard et al.* [1999] and will be used here to estimate the gouge compaction and crack sealing rates. Three types of parameters are needed in such a law: the nature of fluids and minerals, the geometry of the mass transfer path (width and length), and the kinetics of the mass transfer processes (kinetics of reaction, mass transfer flux along trapped fluid path). The first two are derived by observing the nature of the mobile species and the geometry of sealed cracks and solution cleavage near the faults; this was the goal of the present work. The third ones are obtained from previous experimental results.

3. Moreover, mass transfer along trapped fluid phase is a required step even when the fluid phase is mobile (infiltration) since the dissolved species has to be extracted from the loaded faces. In this case there are four successive steps: dissolution, diffusion away from the trapped water-film fluid, fluid infiltration transport, and deposition. The problem is thus to identify the source of the matter (the dissolution zone along the infiltration path). If this source is made up of cavities or a free surface (Figure 1c), then the limiting process is, most often for low solubility minerals, either the rate of reaction at the solid/fluid interface or the infiltration process. If this source is a pressure solution cleavage (Figure 1c), then the limiting process is, in most cases at depth in the upper crust (deeper than 3 km for quartz), the diffusion mass transfer step along the solution surface [*Renard et al.*, 1997].

[10] Consequently, observations of natural pressure solution processes near active faults give several indications on mechanisms and parameters required for modeling crack sealing. However, since it is not currently possible to sample at depth near active faults, the only way to study the crack sealing processes at depth is to collect samples near faults which were active at depth and then uplifted. Consequently, samples were collected near such active faults, with great care being taken in studying only the structures clearly related with the active displacement of these faults at depth prior to their uplift. Using both the geometry of the mass transfer path deduced from these natural observations and experimental results on pressure solution, the kinetics of crack sealing was estimated and used to model the variation in fluid pressure near and within active faults. This was done while simultaneously integrating the change in permeability of the country rocks, gouge compaction, and fluid flow through the fault gouge. Numerical modeling of fluid pressure and fluid transfer around active faults has been performed that reveal different consequences of these three factors and the possibility of discriminating their effects.

3. Observation of Natural Crack Sealing Mechanisms Near Active Faults

[11] Samples were collected from several sites (Figure 2a) near two major faults in California: Little Pine fault and San Gabriel fault that were recently uplifted and exposed. This

sampling was supplemented by collecting country rock samples within the Mother Lode vein system presumed to be associated at depth with fault-valve activity [*Sibson et al.*, 1988]. These various examples allowed observation of crack sealing in rocks brought up from depths of several kilometers. The Little Pine site is in the sedimentary cover, and the San Gabriel sites are in granitoid rocks. The Mother Lode site is in metamorphic schist. Pressure and temperature conditions of crack sealing increase from the first to the last examples (see schematic location in cross section, Figure 2b), giving a sampling of crack sealing processes near active faults through the entire upper crust.

3.1. Little Pine Fault

[12] Examples of dissolution features associated with the progressive opening and deformation of tension gashes have been found in upper Miocene Monterey shale near the Little Pine fault (site 1, Figure 2). This fault, about 55 km long, dipping toward the northeast, shows a reverse displacement. The associated north-south compression began about 4 Myr ago [*Yeats et al.*, 1994; *Molnar*, 1993; *Gratier et al.*, 1999a]. Its most recent rupture occurred during the late Quaternary [*Jennings*, 1994]. Nearly vertical solution cleavage parallel to the axial plane of folds (several tens of meters in size) is found very clearly, up to several hundred meters from the major thrust fault. Fold axes and cleavage are subparallel to the fault direction, reflecting intense shortening more or less perpendicular to this fault direction, thus indicating that these deformations are related to thrust displacement.

[13] Samples obtained a few meters from the fault thrust show nearly vertical tension gashes perpendicular to the solution cleavage in near horizontal strata. These veins were developed and then folded during the progressive deformation of the rocks (Figure 3a). Younger veins are almost undeformed with planar walls whereas earlier veins are tightly folded and show evidence of localized dissolution near large solution cleavage zones. Intermediate fold geometry may also be found, indicating progressive shortening during the formation of the veins.

[14] Three types of healing and sealing processes may be found on the thin sections:

1. Most of the veins are sealed by syntaxial calcite fibers. Such fibers grow from the wall toward the inner part of the vein, the last increment of growth being near a central suture (Figure 3a). Successive openings and sealing processes are revealed by the difference in color along the fibers (Figure 3a). Crack seal events are shown by stripes of specific color parallel to the wall of the vein and they affect the entire vein. The large aperture of each successively sealed crack (from 10 to 100 μm), which is associated with a clear input of material, is incompatible with a self-healing process alone. The veins are systematically associated with solution cleavage (Figure 3b) which appears as axial plane cleavage of the folded veins. Some veins are interrupted, by dissolution, against solution cleavage (Figure 3a). Owing to the progressive shortening of the rocks, lateral dissolution of the vein fibers clearly appears as solution seams. So, most of the sealing process is associated with stress driven diffusive mass transfer.

2. In some cases, the last opening of certain veins was large enough to break the continuity of the fiber growth by successive increments of fracture and sealing. This leads to a change in the style of precipitation. Euhedral calcite crystals are found in this case (Figure 3c): this is indicative of large and permanent openings, which may have been associated with fluid infiltration. Finally, quartz minerals seal the remaining voids.

3. In the vein crystals, fluid inclusion trends may be interpreted as healed microcracks posterior to the sealing process (Figure 3d).

[15] The shortening perpendicular to the cleavage may be estimated by unfolding the earlier veins (Figure 3a). This shortening reaches a minimum mean value of 30% over tens to hundreds of meters along the outcrop. The elongation value indicated by the veins is only about 1–2% at the same scale. So it is interesting to estimate the mass transfer balance from solution cleavage to veins. Solution cleavage is well developed in the matrix near the most rotated microfold limb veins. Consequently, tectonic layering develops perpendicular to the pre-existing sedimentary layering (Figure 3e). Mass change and mobile elements associated with pressure solution tectonic layering can be estimated by comparative chemical analysis assuming insoluble species to be passively concentrated in sectors where soluble species are removed. The best way to test this assumption is to plot the change in chemical analysis through the tectonic layers [*Gratier*, 1983]. Core samples have been taken in the same sedimentary horizontal layer near a vertical folded vein (Figure 3e). The sampling area ranges from zones of maximum shortening (near the most rotated microfold limb) to zones of minimum shortening (near the less rotated microfold limb). The ratio of content of each element in the exposed zone (samples 3 and 4) versus the content of the same element in the protected zones (samples 1–2–5–6) is plotted in Figure 3g (left). This ratio is normalized relative to the Al content. Two elements follow the same behavior (Al, Ti) and may be considered as insoluble and two others are not far from them (Fe, K). On the contrary, other elements such as Ca, Si, loss on ignition (PF) exhibit the behavior of mobile species, while P and Mg exhibit intermediary behavior. As some elements (i.e., Si), may belong to both soluble and insoluble minerals, it is convenient to express mineral content of the samples. The presence of minerals was detected by XRD analysis (quartz, calcite, dolomite, and kaolinite), minor minerals being seen in thin sections as Fe Ti oxides. The mineral content was calculated using the oxide content (Figure 3g, right). For simplicity, the mean behavior in the zone of maximum density of solution cleavage seams (exposed samples 3 and 4) is compared to all the other parts of the layer (protected samples 1–2–5–6). The total mass change $\Delta M/M$ between a given (exposed) sector and the reference (protected) sector is given by a simple relation [*Gratier*, 1983]:

$$\Delta M/M = \left(I_p/I_e\right) - 1, \tag{1}$$

I_p and I_e being the percentage of insoluble minerals in the exposed zone (I_e) and in the protected zone (I_p).

1. When only kaolinite is considered as insoluble mineral, the total mass change between the protected and

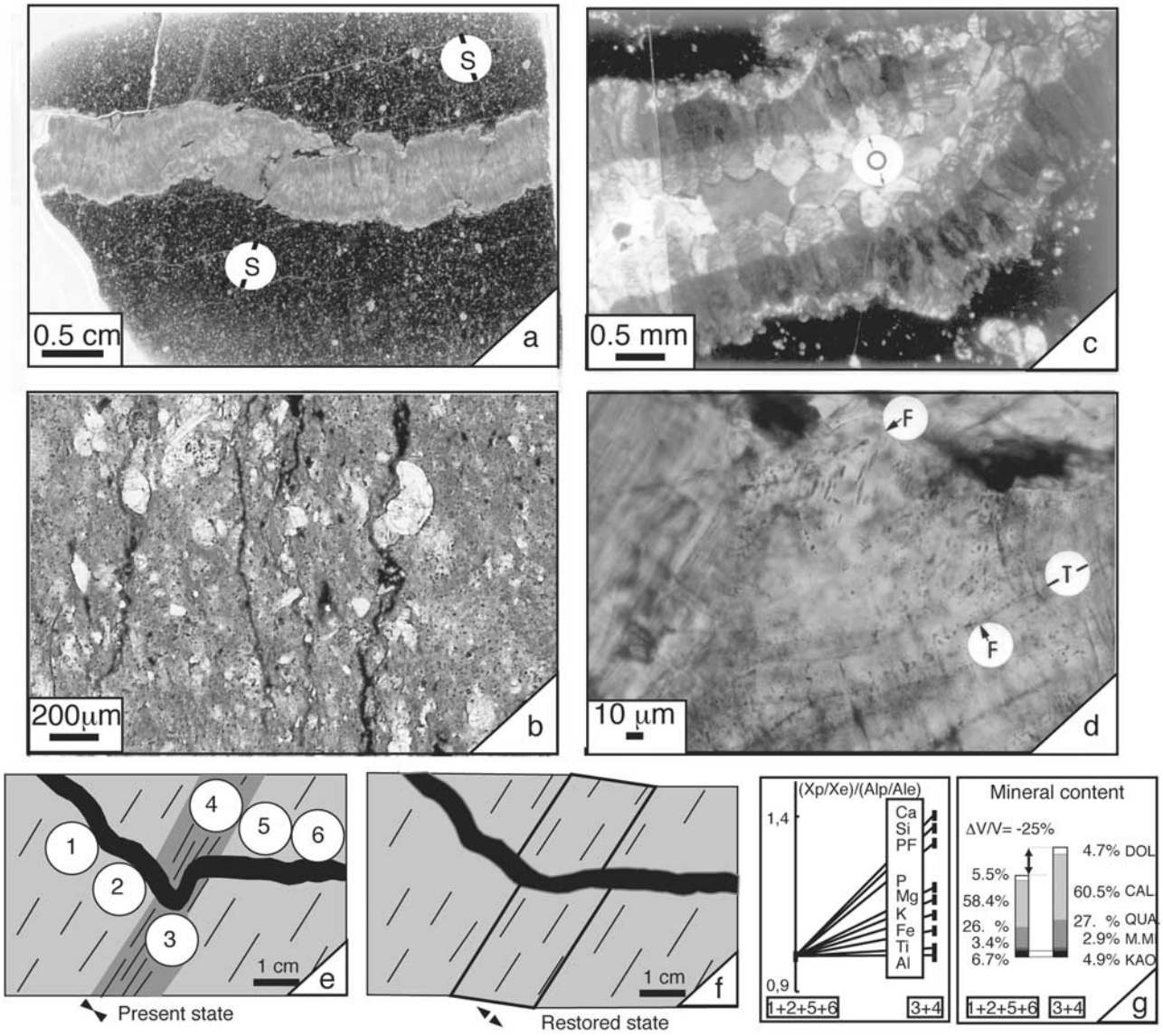

Figure 3. Deformation microstructures in country rocks near the Little Pine fault (site 1) in Monterey Miocene shales indicating horizontal shortening nearby active thrust fault and related to interseimic creep and compaction processes. (a) Mass transfer from solution cleavage (S) to veins. Youngest veins are almost undeformed and perpendicular to the solution cleavage, whereas earliest veins are tightly folded and locally dissolved. (b) Detail of solution cleavage. Passive concentration of insoluble species (black) marks the spaced solution seams (vertical). (c) Detail of veins with local voids filled by euhedral crystals of calcite (C) and latter filled with quartz (Q). (d) Trails of fluid inclusions (F) indicative of the crack healing process in the minerals of the veins. (e) Location of samples used for calculation of mass transfer and (f) restored state using the estimated volume change. Drawing is a map view; vertical tectonic layering (shaded area and solid lines) and folded veins (black area) are perpendicular to the horizontal stratification. (g) Calculation of mass transfer associated with pressure solution: X_p/X_e is the ratio of oxides content between minimum shortening zones (1 + 2 + 5 + 6) and maximum shortening zones (3 + 4). Al_p/Al_e is the specific ratio for Al. Comparison of mineral content between the two zones is given on the right part with volume decrease of zone (3 + 4) versus zone (1 + 2 + 5 + 6) by pressure solution.

the exposed sectors is −27%. The mass decrease of each soluble mineral $\Delta M_m/M_m$ is

$$\Delta M_m/M_m = \left(I_p/I_e\right)\left(M_e/M_p\right) - 1, \qquad (2)$$

M_e and M_p being the percentage of each soluble mineral in the exposed sectors (M_e) and protected sectors (M_p), the relative change in mass of each soluble mineral is −15% for dolomite, −30% for calcite, and −30% for quartz.

2. When both kaolinite and all minor minerals are considered as insoluble minerals, minimum mass decrease values are obtained: the total mass decrease is −23% and the relative mass decrease is −10% for dolomite, −26% for calcite and −26% for quartz.

[16] Assuming nearly constant density between initial and deformed zones, the mass change is equal to the volume change. This volume change can be used to restore the deformation associated with the partial unfolding of the vein (Figure 3f). An approximate 10% global decrease in volume is estimated from this restoration, accommodated by the shortening perpendicular to the tectonic layering. When comparing this shortening value with the 30% shortening found by unfolding the earliest veins, mass transfer at this centimeter scale only accounts for part of the shortening. Deformation also occurred at matrix scale by stylolites, grain dissolution and grain sliding (Figure 3b). Consequently, the geometry of the mass transfer path under stress, which is a crucial parameter in the creep law (see section 1), is measured at granular scale on thin sections.

[17] Rheological parameters of the rocks may be estimated directly from finite deformation analysis. When considering pressure solution creep as a Newtonian viscous flow, the strain rate is proportional to the shear stress and inversely proportional to the viscosity coefficient. Constant strain rate is derived from true finite strain [*Pfiffner and Ramsay*, 1982]. Assuming a total duration of 4 Myr (see above) and a mean differential stress value of 20 MPa [*Gratier*, 1987], the viscosity coefficient is estimated to be equal to 8×10^{21} Pa s. This is a maximum value since pressure solution creep may be limited to a short period after each earthquake (see discussion).

[18] Mass transfer balance indicates that the local amount of dissolution is greater than the amount of precipitation. The extent of the precipitation zone has encompassed more than just the zone containing the solution cleavage (several hundred meters in extent). Consequently, at least part of the soluble species removed along the solution cleavage must have been transferred out of the shales by infiltration and may have contributed to sealing the veins in the nearby country rocks (sandstones, serpentines, etc.). However, as mentioned in section 2.2.3, the kinetics of the sealing process is most often controlled by the stress-driven diffusion-controlled step.

3.2. San Gabriel Fault

[19] The displacement on the San Gabriel fault was primarily a right lateral strike slip. The most recent ruptures occurred during Quaternary times [*Jennings*, 1994; *Petersen and Wernousky*, 1994]. Recent uplifting of the San Gabriel Mountain along thrust faults (i.e., the Sierra Madre fault) exposed outcrops of crustal levels that were previously lying at a depth of 2–5 km [*Jennings*, 1994]. Microstructures and mineral assemblage of the fault rocks observed on such outcrops are consistent with faulting at these depths [*Chester et al.*, 1993; *Evans and Chester*, 1995].

[20] Mass transfer and fluid/rock interactions within the fault gouge have been studied in detail by *Chester et al.* [1993] and *Evans and Chester* [1995]. They found evidence of chemical differentiation between the gouge and the host rocks. The ultracataclasites of the gouge are rich in Fe, Mg, Mn, and Ti relative to the composition of the protolith, this observation being interpreted as a fluid assisted process with volume loss of about 37%. This chemical differentiation is considered to be the result of mechanical mixing with local redistribution of some elements in contact with the fluid, with either open or closed systems depending on the sites.

[21] The aim of our study, which is complementary to this preceding work, is to consider the different mechanisms and rates of crack sealing mainly in the country rock near active faults. Samples were collected from outcrops several meters to hundreds of meters from the central gouge zone of the San Gabriel fault (in granites and metamorphic rocks; site 3, Figure 2). In addition, samples were taken directly within the San Gabriel fault gouge (site 2, Figure 2). Structures in thin sections (Figures 4 and 5) give the main displacement and the principal deformation features. A typical cataclastic process accommodated the fault displacement. Secondary fractures near the narrowest cataclastic zone were developed either as conjugate fractures or as Riedel fractures (R, Figure 5a).

[22] Away from the main gouge (site 3, Figure 4), the crack orientation (T) indicates the direction of shortening, and ranges from 020° to 045° with respect to the faults. This variation may be related to the heterogeneous state of stress or to the rotation/distortion of some of the blocks. Quartz is the mineral most frequently filling the sealed cracks. However, a network of very thin veins, filled with calcite, is seen by cathodoluminescence studies and is the latest episode of crack sealing. Dissolution features can be distinguished in the samples. The sealed cracks (T) are associated with and are perpendicular to solution cleavage (S in Figures 4a, 4b, and 4c). Most of the veins are interrupted against solution cleavage this relation indicating their closed relationship (Figures 4a and 4c). This solution cleavage can be seen at the scale of several grains (stylolites, Figure 4c) or at the scale of a single grain boundary (Figure 4b). Figure 4d shows schematic restored state of Figure 4c (before dissolution along stylolites) with location of the transgranular dissolution zone and the associated veins which are interrupted against this dissolution zone. The mean spacing between microcracks gives the size of the elementary trapped fluid area which will be used in the pressure solution modeling [*Gratier et al.*, 1999b]. Most structures show a spacing ranging from 50 to 500 μm. Quartz and feldspar both show evidence of dissolution under stress as found in the same context in other regions [*Kirkwood et al.*, 1999]. The crack aperture (or at least the thickness of the filling material) is easy to estimate when the sealing mineral is different from the host mineral (Figures 4a and 4c). Crack apertures range from 10 to 100 μm. Apertures are more difficult to estimate when the sealing and the host mineral are not easily differentiated. An example of transgranular cracks through an inclusion in quartz (Figure 4b) shows that the two limits of the cracks are often underlined by two trails of fluid inclusions in the host mineral. Contrary to some of the veins in the Miocene shale (which show successive micro-opening and sealing events), each of the fractures within the San Gabriel fault appears to have been opened and sealed only once.

[23] Within the San Gabriel fault gouge (site 2, Figure 5), some special features seem to appear in decimeter-sized blocks. Mica minerals coat the limits of the secondary fault gouges (M, Figure 5b). The growth of these minerals is also observed in pressure shadow zones around large quartz grains (Figure 5b). These features indicate that along some mass transfer paths, hydrothermal or metamorphic reactions may have contributed to a reduction in permeability [*Wintsch et al.*, 1995]. However, these reactions are limited

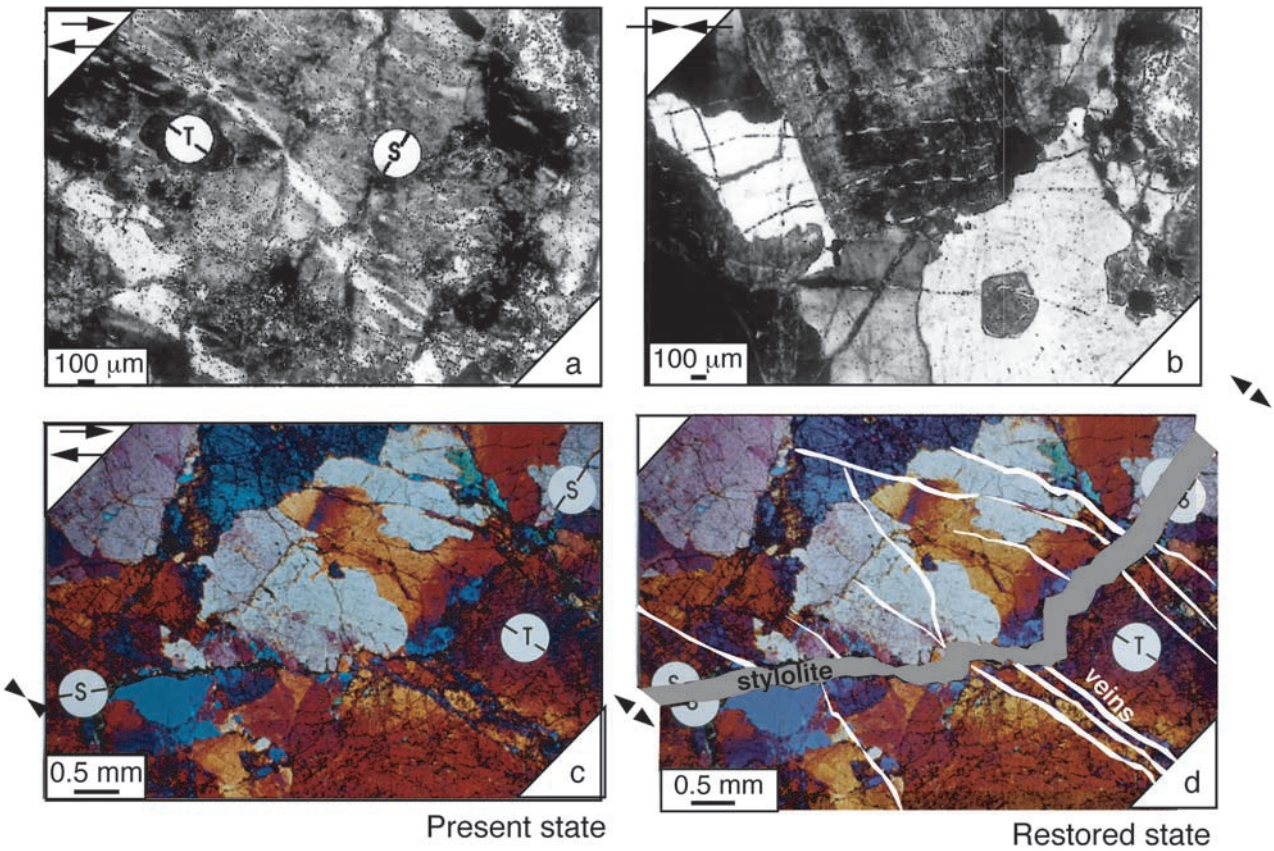

Figure 4. Deformation microstructures in country rocks near San Gabriel fault (site 3) in granitoid rocks indicating shear deformation parallel to active strike-slip fault and related to interseimic creep and compaction processes. (a) Mass transfer from solution cleavage (S) to veins (T) in quartz and feldspar. (b) Network of sealed cracks. (c) Mass transfer from stylolites (S) to veins (T), and (d) restored state (before sealing) with dissolved area (gray) and open cracks (white area).

for the most part to areas associated with large fracture systems that have not been completely sealed. These types of reactions have been related to external fluid flow in some of the studied sites [*Chester et al.*, 1993].

[24] After cataclastic processes took place in the fault gouge, there is also evidence of compaction by pressure solution. Solution cleavages are found (S, Figure 5c) in fault gouges. Equidirectional indentation of some grains by others, due to compaction by pressure solution, is also seen in the main gouge, as well as in secondary gouges in the country rock (S, Figure 5d). Evidence of undulated extinction revealing local plasticity is observed, but indentation is not always associated with such structures. Partitioning of the deformation mechanisms has thus been observed within the gouge where most of the compaction is attributable to pressure solution. Such a volume reduction can be associated with the temporary variation in fluid pressure during the seismic cycle (from near lithostatic before an earthquake to near hydrostatic values after an earthquake).

3.3. Mother Lode Valley

[25] The Mother Lode fracture system comprises numerous veins distributed in and around the Melones fault zone [*Knopf*, 1929]. This fault zone, which dips steeply (70–90°), lies within the western metamorphic belt of the Sierra Nevada, as part of the Foothill fault system, parallel to the San Andreas fault zone. Typical Mother Lode veins and associated subsidiary features are schematically shown in Figure 6a [after *Sibson et al.*, 1988]. Arrays of subhorizontal veins (flats) develop adjacent to the major fault-vein. Textural evidence suggests that both fault filling and flats developed incrementally in broad contemporaneity. Identical vein assemblages are found in other mesothermal vein systems developed in granite-greenstone terrain [*Robert and Kelly*, 1987; *Boullier and Robert*, 1992; *Cox et al.*, 1991]. Such systems have been interpreted as being linked to fault-valve processes developed during earthquake cycles [*Sibson et al.*, 1988]. In the Mother Lode, fluid inclusions and stable isotopes indicate the range of temperature (250–325°C) and pressure (100–200 MPa) of the mineral deposition [*Bohlke and Kistler*, 1986; *Weir and Kerrich*, 1987]. The grade of metamorphism suggests a depth of about 7–10 km [*Bateman and Eaton*, 1967]. The vein system is interpreted as representing rupture nucleation sites developed at depth near the base of seismogenic zones [*Sibson*, 1992a]. Sulphide-rich zones and gold mineralization associated with the Mother Lode vein system imply large amounts of aqueous fluid flowing through the fault zone from depth. However, not all the quartz veins carry a

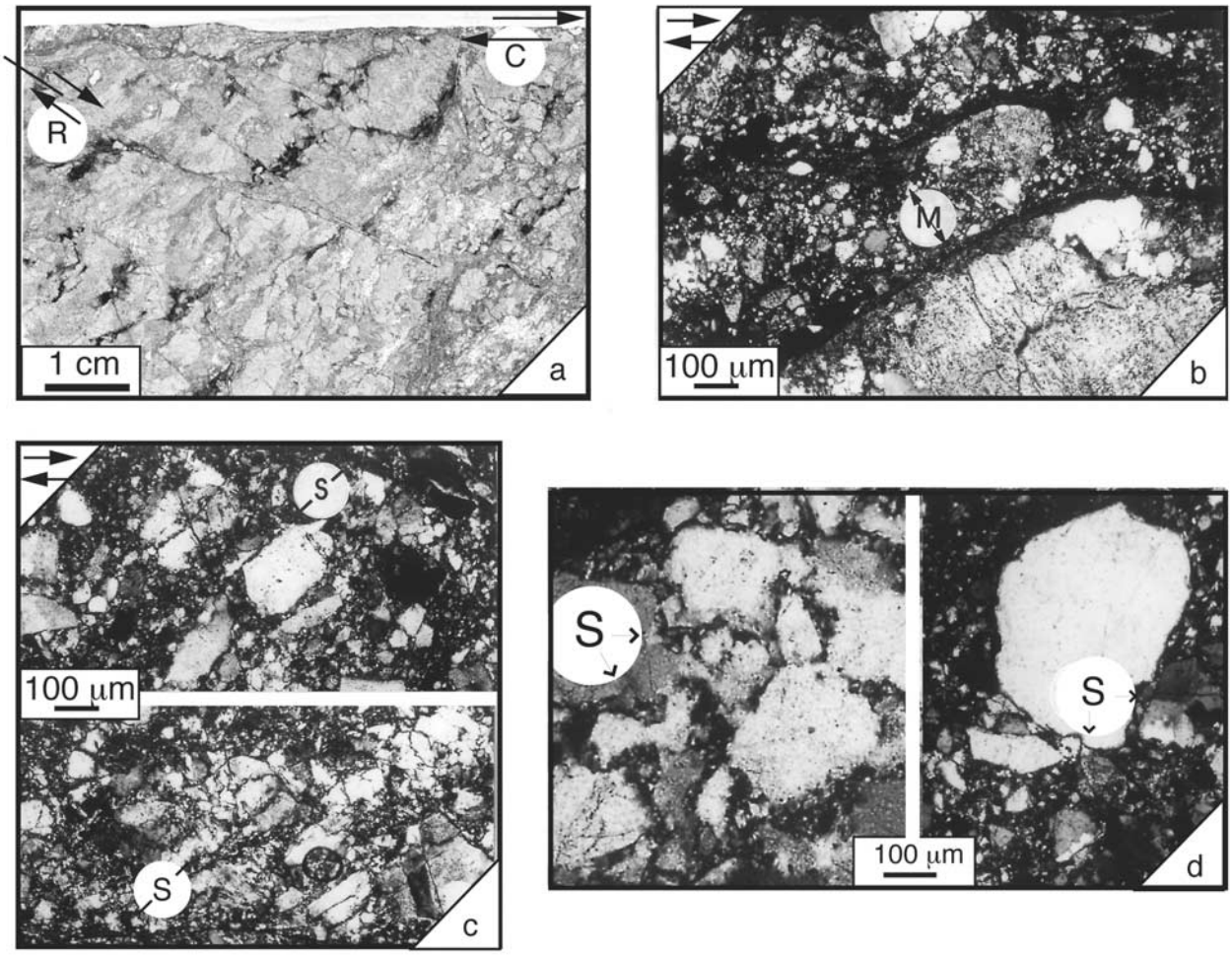

Figure 5. Deformation microstructures within the San Gabriel fault (site 2) in granitoid rocks indicating shear deformation parallel to active strike-slip fault and related to interseimic creep and compaction processes. (a) En echelon strike slip fractures (Riedel fractures, R) near the boundary of the fault gouge (C). (b) Mica growth along the infiltration path within the San Gabriel gouge. (c) Solution cleavage within the gouge compatible with aseismic strike-slip displacement. (d) Markers of gouge compaction by pressure solution, pits in all directions (S).

significant gold value and solution cleavage is found all around the fault system (Figures 6b, 6c, and 6d). As for the San Andrea veins, it is thus pertinent to investigate mass transfer from solution cleavage to veins in order to estimate the mechanism of crack sealing in the country rocks near the main fault. The vertical NW-SE trending solution cleavage attests to the NE-SW horizontal shortening. Its development is compatible with the reverse fault displacement. In thin sections the vertical solution cleavage is associated with the development of tectonic layering perpendicular to the initial horizontal bedding (Figures 6b and 6c). Insoluble minerals (mainly micas) are passively concentrated in the dissolution zones. Evidence of stylolitic surfaces is found along the (vertical) boundary of rigid elements exposed to maximum stress values (horizontal shortening) (Figure 6c). The sealed cracks are filled mostly with quartz but also with calcite (Figure 6d). Synchronous growth of these two minerals can be seen, regardless of how the successive filling episodes may be depicted. As in the preceding examples, sealed cracks may be found either cut by dissolution zones (Figures 6b and 6c), or interrupted against the dissolution zones (Figure 6d) even for large veins (several centimeters wide). This indicates the simultaneous development of dissolution features and crack sealing.

[26] Mass loss and mobile elements can be found from comparative chemical analysis. Map distribution of various elements (Figure 6e) shows the difference between mobile species (Si, Na) and immobile ones (Al, K). Si is mostly present in quartz, micas and feldspars, Na is mostly in feldspars, and K and Al are mostly in micas. Profiles of chemical element analysis have been acquired perpendicularly to the dissolution zones and parallel to the strata (Figure 6f). In order to assume an initial constant chemical composition along the strata, the heterogeneity of the rock is smoothed by integrating the chemical composition over a width of 200 μm. This was done by successive analysis of contiguous areas of 12×200 μm. As previously, the change in Al content can be considered as being well representative of the behavior of the insoluble minerals passively concen-

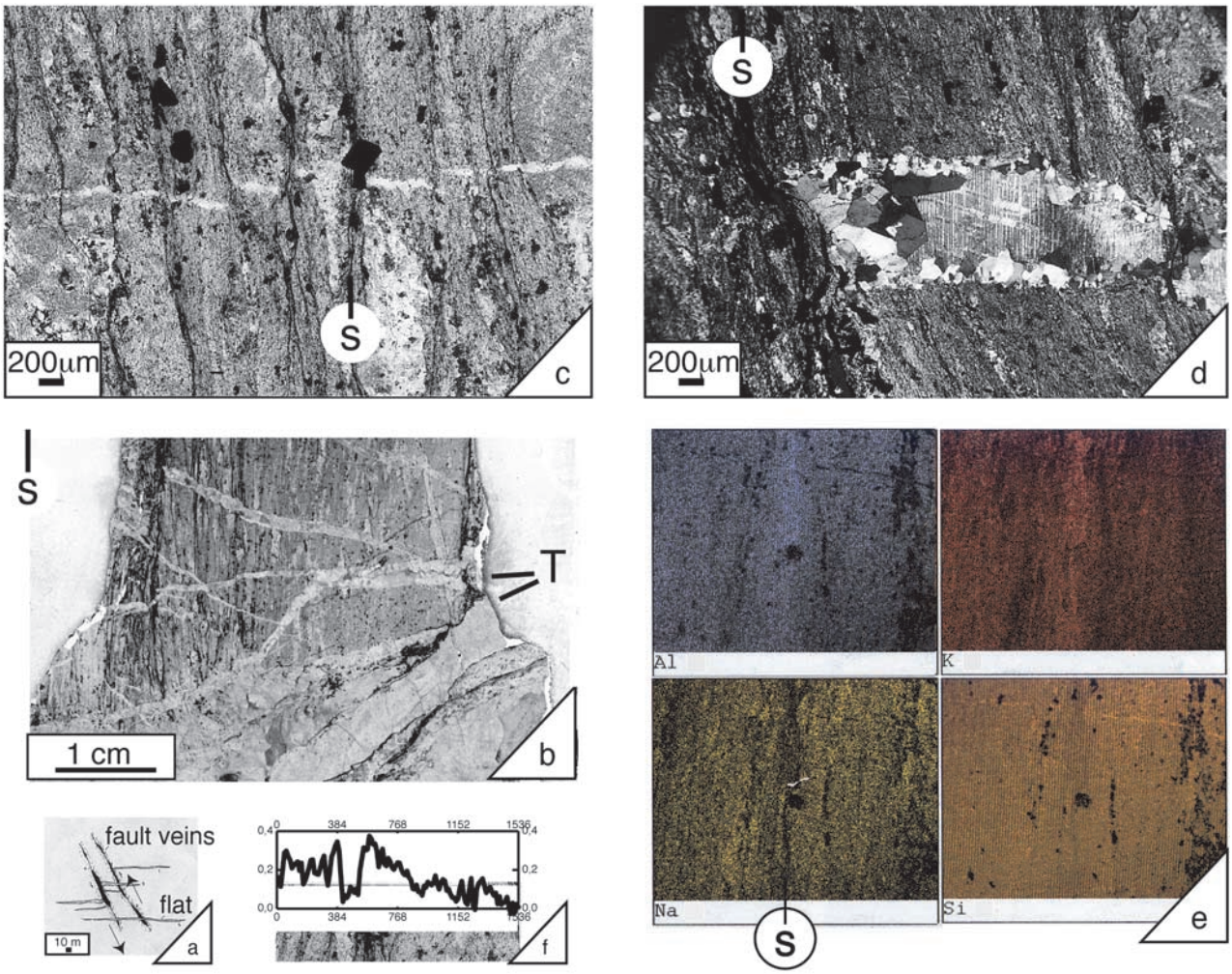

Figure 6. Deformation microstructures in country rocks near the Melones fault (Mother Lode valley), site 4, in metamorphic schist, indicating progressive deformation compatible to the nearby active fault and related to interseimic creep and compaction processes. (a) General settings of the fault-vein system along vertical cross section [*Sibson et al.*, 1988]. (b) Thin sections of metamorphic rocks (site 4) mass transfer from solution cleavage (S) to veins (T). The initial stratification is horizontal. (c) Detail of solution cleavage seams crosscutting the veins by dissolution. (d) Detail of the ending of a vein (filled with both quartz and calcite) against a solution cleavage seam (S). (e) Distribution of the content of some elements. Na and Si show a depletion in solution cleavage (S) reflecting their dissolution, whereas Al and K show an increase in content in solution cleavage due to their passive concentration in the dissolution zone. (f) Relative decrease in volume: $\Delta V/V = \Delta M/M = (I_p/I_e) - 1$, through solution cleavage seams (deduced from Al concentration profile, I_e) with respect to a reference zone (zones of lowest Al content, I_p). The initial stratification is horizontal.

trated in the zones of dissolution. Assuming constant density during deformation, the total volume loss along the profile is obtained by integrating the volume loss associated with each incremental area of measurement (Figure 6f):

$$\Delta V_t/V_t = \Delta M_t/M_t = \Sigma_1^N \left[\left(I_p/I_e\right) - 1\right]/N, \qquad (3)$$

where N is the number of successive incremental areas of analyzed rocks, I_p and I_e are the Al content in a reference zone and in the successive incremental analyzed stripes of rocks, respectively. The composition of the reference zone is of crucial importance. We choose the right part of the profile in a zone of 72 $\times$ 200 μm, without any visible trace of redeposition. The calculation gives a global volume depletion of −15.6%, accommodated by the shortening perpendicular to the cleavage. Consequently, at least part of the mineral deposited in sealed cracks clearly comes from nearby solution cleavage. This is demonstrated for veins up to several centimeters wide (Figure 6b). Above such a width the relation between solution cleavage and deposited mineral is less clear. However, metamorphic rocks near the fault clearly show volume loss and mineral depletion in the same species that are found in the large veins. As for Little Pine, −15.6% shortening is a minimum value for the total shortening perpendicular to solution cleavage since

mass transfer by pressure solution deposition also occurs at a smaller distance (grain size).

4. Crack Sealing and Compaction Modeling Around Faults

4.1. Basic Element Deduced From Fault Processes Analysis

[27] The main characteristics of the observed natural structures may be summarized as follows. Fluid inclusion networks in the mineral of the veins reflect the presence of fluid during the sealing of the cracks. The veins related to active faults are always sealed with input of mineral. Mineral deposits in veins are mostly removed from nearby solution cleavage and stylolites in country rocks. This can be demonstrated both by geometric arguments (veins interrupted against solution surface) and by chemical arguments (same mineral dissolved in solution cleavage and redeposited in veins). Dissolution interfaces are oriented perpendicularly to σ_1 and fractures are opened perpendicularly to σ_3. Such orientations are in agreement with a stress gradient driven mass transfer namely pressure solution. Therefore we consider that pressure solution deposition is the main mechanism of crack sealing around active faults. Within the gouges, the growth of some minerals is indicative of metamorphic reactions with external fluids. However, systematic compaction occurred in the gouge after the seismic cataclastic process, mostly by pressure solution.

[28] Quartz and calcite are the main mobile minerals, which are removed from the stylolites and redeposited in veins and pores. However, the relative mobility of quartz and calcite clearly changes with depth. At smaller depth, calcite is more mobile than quartz while the reverse is true at greater depth. This variation is related to two converging effects: (1) the solubility of quartz and calcite vary inversely with increasing temperature (normal and reverse relation respectively for quartz and calcite) and (2) at low temperature, the kinetics of quartz dissolution is very low and this prevents significant pressure solution process [*Oelkers et al.*, 1996; *Renard et al.*, 1997].

[29] The theoretical variations in the strain rate of quartz and calcite aggregate versus depth are given by *Rutter* [1976], *Gratier* [1987], and *Renard et al.* [2000]. This variation shows that an equal strain rate may occur at about 180–220°C and 100–200 MPa, depending on the geothermal gradient (50–30°C km^{-1}).

[30] The origin of the fluids in fault systems can be estimated from isotope studies. Mantle signature, from $^3He/^4He$ ratios studies, was revealed by *Kennedy et al.* [1997], in the present-day groundwaters associated with the San Andreas system. More recently, the isotope composition of gouges and vein filling minerals have been compared with host rocks by *Pili et al.* [1998, 2002]. This study allowed the past fluids flowing through the San Andreas fault system to be identified. Hundreds of samples from over 25 localities along the SAF and adjacent faults from south San Francisco to east Los Angeles were analyzed. Samples from the exhumed San Gabriel fault and Little Pine fault were also included. Many lithologies (granites, sandstones, limestones, marbles) were sampled for isotope analyses of carbon, oxygen, helium and other noble gases. *Pili et al.* [1998] show that the C and O isotope analyses of carbonates from gouges, vein fillings and their host rocks form a consistent trend suggesting percolation of external fluids. Ranking in terms of decreasing isotope depletion, and thus decreasing deep-fluid signature, would give the gouges, the vein fillings and the host rocks, respectively. Mantle helium signatures have also been evidenced in fluid inclusion from gouges and veins. From these results, fault zones at a given depth (2–5 km) appear to have been infiltrated during deformation by fluids of deeper origin dominated by crustal water with mantle contribution. Meteoric water does not represent a significant contribution. Such isotopic signatures indicate that the fluids, which were not in equilibrium with the host rocks, flow through the entire gouge and the vein system. However, to explain their more marked deep-fluid signature, the gouges must have been infiltrated several times whereas veins were mostly open and sealed once. This is compatible with our observation that part of the mineral matter of the gouges and most of the vein filling mineral material is actually derived from the country rocks. From time to time, probably after earthquake occurrences, gouges and veins are connected together, then, during interseismic period, crack sealing occurs by input of mineral mostly removed from nearby country rocks by pressure solution stress-driven processes. This type of crack-sealing model is also compatible with the results of other authors. For example, within the Kodiak convergent prism, Alaska, *Fisher et al.* [1995] found no evidence for long-distance transport of silica based on regional variations in the chemical composition of slate samples. However, they found geochemical evidence of local migration of silica from the rock matrix to veins with a degree of matrix rock depletion comparable to the amount of quartz precipitated in veins [*Fisher and Brantley*, 1992].

[31] Consequently, according to the observation of natural structures, the following successive crack sealing processes are expected to occur in Californian active fault zones during interseismic periods (see Figure 7a). Initially, an earthquake will serve to increase the overall permeability and reduce fluid pressures to levels approaching hydrostatic values within the fault zone. The first stages of fluid/rock interactions can be characterized by rapid kinetics depending on the reactions taking place on free faces (see section 2). Self-healing of the fractured mineral and some metamorphic reactions are relevant to this stage. However, none of these processes is observed to be associated with efficient sealing of the open cracks. The second stage, involving pressure solution creep, associated with the grain indentation and water-film diffusion under stress, is found to be much more efficient and can be assimilated to a mechanism that relaxes the stress around the fault after each earthquake. It also decreases the effective stress imposed on the matrix because of the decrease in pore pressure between the individual grains after each earthquake, leading to the compaction of the gouge. According to experiments [*Gratier and Guiguet*, 1986], the kinetics of such crack sealing, controlled by the kinetics of pressure solution-deposition processes, is very slow. Modeling such changes is done below. It implies knowledge of the variation in geometry of the mass transfer path. Two schematic variations have been considered:

1. In grain compaction modeling within the gouges (Figure 7b), pressure solution occurs by dissolution at grain

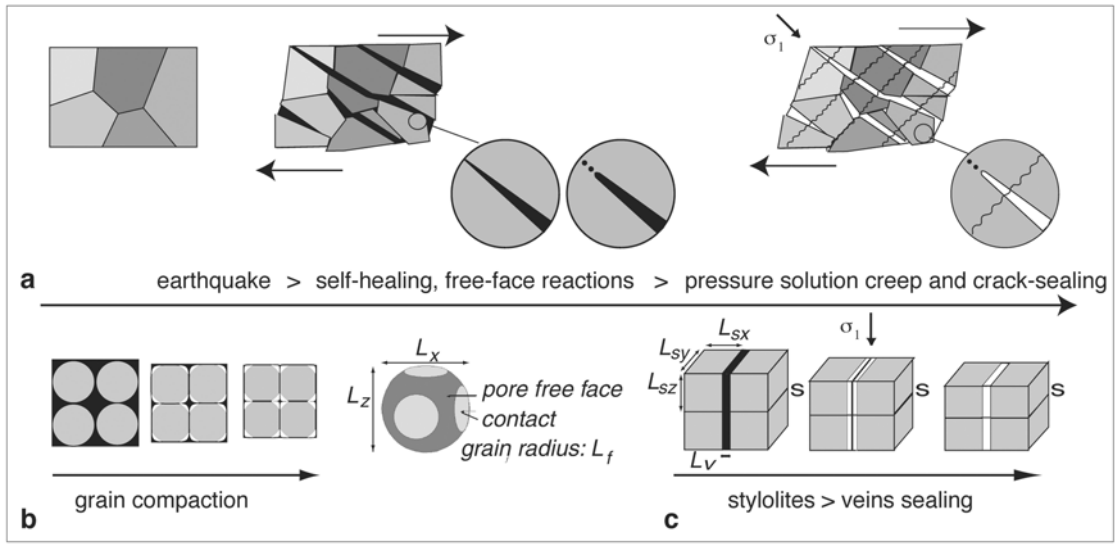

Figure 7. (a) Schematic view of the deformation around fault and crack sealing processes during seismic-aseismic cycle. Time-dependent variation from left to right. First, microcracks develop during earthquake and are filled with fluid (black area). Then free-face reactions occur rapidly; only special conditions lead to the sealing of cracks at this step. At the same time, a fast self-healing process reduces the permeability of the thinnest microcracks (a few microns in width). Finally, progressive sealing occurs by mass transfer from solution cleavage (perpendicular to the maximum compressive residual stress, σ_1) to sealed cracks (white area). Mass transfer also accommodates the creep, which progressively relaxes the stress. (b) Model of gouge compaction by truncated spheres. (c) Model of creep and crack sealing.

contacts and precipitation of the dissolved matter in the pore space. By this mechanism, grains indent in each other and the overall porosity decreases

2. In crack-seal and creep modeling around the faults, mass transfer takes place between dissolution surfaces (i.e., stylolites), perpendicular to the maximum compressive stress direction and precipitation occurs in open cracks (Figure 7c).

[32] Such modeling must integrate two main characteristics: (1) nonlinear dynamic process arises from the fact that during deformation dissolution contact areas grow, consequently the ratio between local stress and regional stress values changes during progressive deformation; and (2) the kinetics of the entire process is dependent on the kinetics of successive ''in series'' steps: dissolution, diffusion, precipitation; when considering the entire crustal condition, each of these processes can be the slowest limiting process.

[33] A unified transitional pressure solution model has been developed by *Renard et al.* [1999] and is used here. This incorporates both the nonlinear stress-geometry relation and various limiting steps, either diffusion rate or reaction rate (precipitation).

4.2. Compaction and Crack Sealing Modeling

[34] The driving force for mass transfer by pressure solution is the difference in chemical potential $\Delta\mu$ between the dissolution sites and the deposition sites. This difference can be written [*Gibbs*, 1877; *Paterson*, 1973; *Shimizu*, 1995]

$$\Delta\mu = \Delta f + \overline{V}_s \Delta P_n, \tag{4}$$

where Δ denotes differences from reference states and P_n is the normal stress on the solid. The term Δf contains contributions due to elastic energy, dislocation energy, and surface energy.

[35] 1. For grain compaction in the gouge, the rock is modeled as a cubic array of monomineralic grains [*Dewers and Ortoleva*, 1990b]. The grains have a truncated spherical geometry (Figure 7b). Isotropic loading of the system is assumed, with the transfer driving force being the difference between lithostatic pressure and hydrostatic pressure. For simplicity, only the deformation in one direction (z) is explained here. In this case, two velocities G_c and G_p (m s^{-1}) describe the geometric change in the z-contact length variables. G_c is representative of the time-dependent change in the moving grain interface due to dissolution at contact, and represents the rate at which L_z decreases with time. G_p takes into account the change in grain radius due to precipitation and characterizes the overgrowth thickness on the pore surface. The detailed description of the model is given by *Renard et al.* [1999] and will not be detailed here. For the diffusion limiting process, Fick's law gives

$$\frac{2\pi l_c \Delta D_c (c_c - c_p)}{l_c} = -\frac{A_c}{\overline{V}_s} G_c, \tag{5}$$

where A_c is the surface area of the contact; c_c and c_p are the concentrations inside the contact and in the pore fluid, respectively, the difference in solubility is related to the driving force (stress difference) by a steady state assumption through the difference in chemical potential [*Dewers and Ortoleva*, 1990a]; $\overline{V}_s$ is the molar volume of the dissolving solid; D_c is the coefficient of diffusion through the grain boundaries; Δ is the thickness of the interface; and l_c is the radius of the circular grain contact. Volume conservation is assumed at granular scale: $6A_cG_c + A_pG_p = 0$.

For the interface reaction limiting process (precipitation), the rate G_p corresponds to the precipitation on the pore surface:

$$G_p = k_p\left(1 - \frac{c_p}{K_{eq}}\right), \tag{6}$$

where k_p is the rate of quartz precipitation and K_{eq} the equilibrium constant for the dissolution/precipitation reaction. The variation of the grain shape parameters (L_x, L_y, L_z) with time controls the porosity. The grains of the rock evolve from truncated spheres (high porosity, see Figure 7b) to cubic grains with no porosity. The kinetics of porosity decrease arises through the velocities G_p and G_c (equations (5) and (6)).

[36] 2. For crack sealing around the faults, dissolution occurs along the stylolite surface perpendicular to σ_1 and matter is transported to two sets of perpendicular veins that are open perpendicularly to the stylolites (perpendicular to σ_2 and σ_3). It is assumed that $\sigma_3 = \sigma_2 = P_f$ (fluid pressure in veins). The mean distance between stylolites L_{sz} decreases with time due to dissolution. During the same period, the open veins progressively close because of precipitation and L_{sx} and L_{sy} increase, whereas the open space in veins L_v decrease (Figure 7). As before, G_s gives the rate of change of the interstylolitic region due to dissolution along the stylolite surface, and G_v is the rate of precipitation inside the veins. For the diffusion limiting process, Fick's law describes diffusion from the stylolite to the veins:

$$\frac{4L_{sy}\Delta_s D_s(c_s - c_v)}{L_{sy}} = -\frac{L_{sx}^2}{\overline{V}_s}G_s, \tag{7}$$

where $\overline{V}_s$ is the molar volume of the dissolving solid, Δ_s is the thickness of the stylolite, and D_s is the coefficient of diffusion of the dissolving solute along the stylolite, c_s is the concentration of dissolved matter in the stylolite, and c_v is the concentration of solutes in the open veins. As before, the difference in solubility is related to the driving force (stress) through the chemical potential. Volume conservation is assumed in a closed system (all the matter is dissolved inside the stylolite and precipitates in the veins). For the interface reaction limiting process (precipitation), the rate G_v represents the precipitation on the vein surfaces:

$$G_v = k_p\left(1 - \frac{c_v}{K_{eq}}\right), \tag{8}$$

where k_p is the rate constant for precipitation and K_{eq} the equilibrium constant for the dissolution/precipitation reaction.

[37] The rock is considered to be either pure quartz or pure calcite aggregate. In the gouge the grain size is equal to 10 μm, and just after an earthquake, the porosity of this rock is high and estimated to be around 10% (Figure 5). In the nearby country rocks (Figures 3, 4, and 6), the initial mean distance between veins and stylolites is taken to vary from 10 to 1000 μm from geological observations ($L_{sx} = L_{sy} = L_{sz}$). Just after an earthquake, the veins are considered to be open, with a thickness L_v varying from 0.6 to 60 μm depending on crack spacing. Given these conditions, the initial fracture porosity of the system is also close to 10% (with two sets of orthogonal fractures perpendicular to the stylolite). Compaction and stylolitization are studied for different geological conditions corresponding to a vertical profile in the fault between 0 and 10 km depth. A temperature gradient of 30° km^{-1} is taken. A specific application to the kinetics of crack sealing and compaction in the San Andreas fault system have been done by *Renard et al.* [2000] and is only briefly summarized here for the two types of sealed structures (gouges and country rocks).

1. In the gouges after an earthquake, the driving force is assumed to be associated with the decrease in fluid pressure (difference between lithostatic pressure on the solid skeleton and hydrostatic pressure of the fluid). The hydrostatic pressure gradient is chosen to be 10 MPa km^{-1}, and the lithostatic pressure gradient is 22 MPa km^{-1}. In this case porosity decreases rapidly with time for both quartz and calcite (Figure 8a). Depending on depth, it takes from 1 day (at 8 km) to 50 years (at 2 km) to close the porosity, with a mean value of about a month at 5 km (Figure 8a).

2. In the country rocks, a constant increase in shear stress with depth is assumed for simplicity. For comparison with gouge behavior, the same increase in the driving force values with depth is assumed (12 MPa km^{-1}). The sealing rate is highly dependent on the spacing of the fractures (Figures 8b and 8c). With mean crack spacing values deduced from observation (100–200 μm), the fracture porosity ϕ_{frac} of the rock decreases much more slowly with time than for the gouge. From an initial value of 10% after an earthquake, porosity decreases to 0% in 10^3–10^4 years for calcite and 10^4–10^5 years for quartz at 5 km (Figures 8b and 8c). These fracture sealing rates are 4 to 5 orders of magnitude slower than for compaction of the gouge. Note that the realistic geometry of the crack network would have implied mixing of all the observed crack spacings (from 10 to 1000 μm). Such models were not calculated. The result would have been a more continuous trend of sealing rates from gouge to veins (with the effect of dense crack network of 10 μm) and a longer duration of the entire process (with the effect of a widely spaced crack network of 1000 μm). Our result may be compared with the result of *Hadizadeh and Foit* [2000], who were able to estimate calcite cementation rates in a brittle fault using Sr/Ca partition coefficients. They found calcite precipitation rates ranging from 1.15 10^{-12} to 3.77 10^{-13} m^3 h^{-1} m^{-2} associated with estimated temperatures ranging from 100 to 250°C. Using their result, the sealing of microcracks of 6 μm width (which are associated with the 100 μm fracture spacing in our model) would take between 1000 and 3000 years, very near our results (1000 years, Figure 8c).

[38] Mass transfer by pressure solution from stylolites to veins may also be expressed as a creep law. Deformation rates change with depth in a different manner for quartz-rich and carbonate-rich rocks due to the reverse dependence of the solubility of these two minerals with temperature (Figure 8d). The viscosity calculated for fractured carbonate-rich rocks, at 2 km, is 6×10^{18} Pa s. This value may be compared with the value found from the study of natural deformation in the same condition (near Little Pine fault):

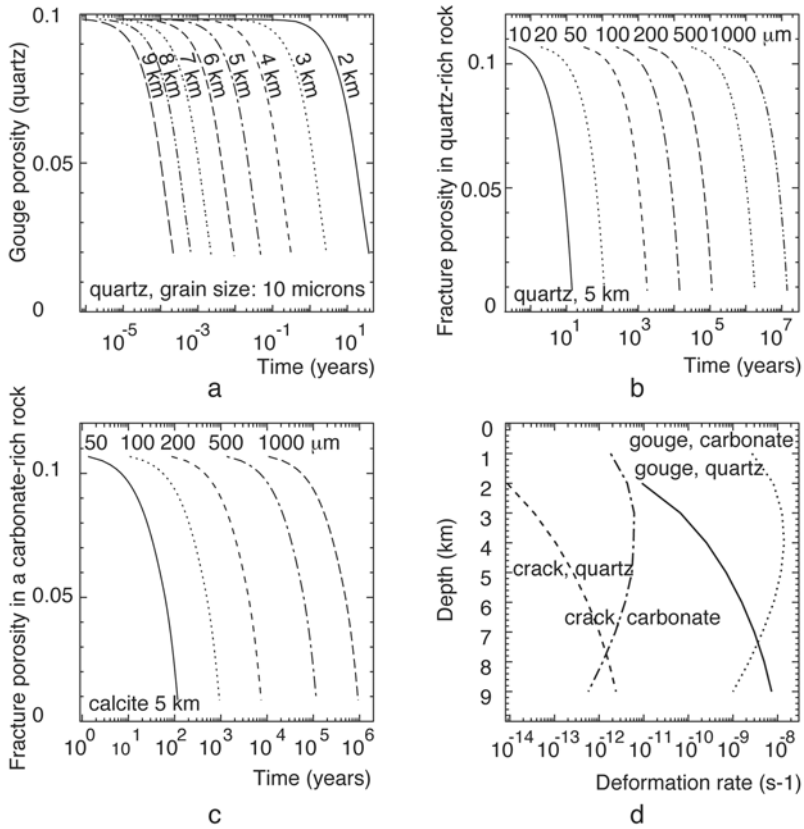

Figure 8. Decrease in porosity of gouge and fractured aggregate with time [after *Renard et al.*, 2000]. The temperature gradient is 30°C km^{-1}. The driving force of the dissolution/deposition process is the difference between lithostatic and hydrostatic pressure for the compaction of the gouge (gradients are taken to be 22 MPa km^{-1} and 10 MPa km^{-1}, respectively). The same change is assumed for the driving force of the crack sealing process (difference in normal stress between stylolites and veins). (a) Calculation of the rate of decrease of gouge porosity after an earthquake, variation with depth, grain size of 10 μm. (b) and (c) Calculation of the rate of decrease of fracture porosity after an earthquake for quartz and calcite, respectively; variations with respect to the spacing between the cracks, from 10 to 1000 μm. The microcrack aperture varies from 0.6 to 60 μm. The depth is 5 km. Notice the log scale for the time axis, in this coordinate, the porosity variations are almost linear, from 10% to 0%, indicating an exponential decrease of the porosity with time. Such a simplified relation was used as porosity decrease model in the numerical modeling of fluid transfer. (d) Variation in mass transfer deformation rate with depth, comparison between carbonate-rich rocks and quartz-rich rocks (gouge and fractured country rocks).

8×10^{21} Pa s. There are several possibilities to explain this difference:

1. The stress value is overestimated in the modeling (but this cannot be associated with 3 orders of magnitude).

2. The spacing between the cracks is underestimated in the modeling (a crack spacing of 10^3 μm is required to fit the natural deformation value). This seems rather high for a mean value.

3. The duration of the natural deformation is overestimated. Instead of considering the total duration of the deformation near Little Pine fault (4 Myr) it could be more convenient to consider that pressure solution creep occurs only during a limited period after each earthquake. Triggered by fracture development, the kinetics of pressure solution shows exponential decrease rates (Figure 8).

[39] These uncertainties could explain the difference of viscosity values when comparing the relatively fast calculated postseismic creep rate and the mean deformation rate for the whole interseismic period. Moreover, the creep rate might include two timescales: very fast strain rate along gouges (months to years) and slower strain rates associated with crack sealing (several years to centuries). This is compatible with geodetic measurements which show large postseismic deformation in the upper crust [*Donnelan and Lyzenga*, 1998].

[40] The progressive decrease in fluid flow through faults must occur concomitantly with the progressive decrease in the postseismic deformation rate due to pressure solution. Two timescales emerge from our calculations: pervasive pressure solution at granular scale on the gouge is much faster than pressure solution along stylolites and precipitation in the veins. So, following this model, compaction of the gouge must be relatively fast but porosity around the fault is maintained for a rather long time. Assuming that the

slower process limits the overall porosity of the fault zone, the change in porosity is modeled only by the crack sealing of veins in country rocks. In such cases, as seen in Figures 8b and 8c, porosity variations are almost linear, from 10% to 0%, indicating an exponential decrease of the porosity with time. Such a simplified relation was used as porosity decrease model in the numerical modeling of fluid transfer presented below. Another problem arises with the crucial difference in behavior between calcite and quartz through the crust. The mobility of quartz and calcite minerals is found to be equivalent at about 4–8 km [*Renard et al.*, 2000; *Gratier*, 1987], depending on the geothermal gradient. However, most of the carbonate-rich rocks are found within the first 2–4 km. Consequently, and in order to simplify, postseismic crack sealing is modeled with a rate of crack sealing that is controlled by pure calcite between 0 and 3 km, by pure quartz between 5 and 10 km, and by an intermediate behavior between 3 and 5 km (Figure 9a).

5. Numerical Modeling of Fluid Transfer Along Active Fault

5.1. Principles of the Model

[41] In order to model the variations of fluid pressure within and around an active fault, a numerical approach has been used which shows the effect of the kinetics of crack sealing in the country rocks around the fault (see Figure 2b for the modeled Californian fault). The basis of the model is relatively simple. A postseismic fluid pressure decrease, down to the hydrostatic pressure, is assumed in a volume limited, at the base of the seismic crust by the lower ductile zone and at the top by the free topographic surface. Laterally, the boundary conditions are considered to be hydrostatic. In the lower crust the fluid pressure remains at a constant lithostatic value when assuming that this part is not fractured during the earthquake process (plastic behavior of the lower crust). Consequently, after each earthquake, the fluid pressure in the fault tends to increase due to the mass transfer from this lower level to the fault zone. This is the source of fluid proposed by [*Rice*, 1992] which progressively increases the fluid pressure from hydrostatic to lithostatic values. The work of [*Pili et al.*, 1998] confirms this assumption for the Californian faults system. The difference between our model and the Rice model is that instead of having instantaneous sealing around the fault, we assume that the permeability within and around the fault slowly decreases with time due to crack sealing and compaction process. This aspect of progressive change in porosity may be matched with the model presented by [*Sleep and Blanpied*, 1992]. However, in their approach, the fluid variation during the interseismic period is modeled as the effect of the change in porosity within the fault gouge but, as in Rice's model, an instantaneous sealing is postulated around the fault (in the country rocks). Consequently, in our model there are two types of processes which may increase the fluid pressure: the inflow of fluid from depth and the progressive change in porosity and permeability by crack sealing within and around the fault. The progressive destruction of the porosity is acquired by the irreversible pressure solution crack sealing mechanism during the interseismic period already described (Figure 7a and 8).

[42] Assumption on the initial porosity profile, just after an earthquake, is of crucial importance for mass transfer modeling. Observation of the natural examples (Figures 3, 4, 5, and 6) shows that fracture porosity (that will be used in the calculation according to the crack sealing model, see above) is highly heterogeneous depending on the nature of the rocks. For example, in the Little Pine site, the porosity of the shales (studied here) is lower than the porosity of the neighboring serpentines. However, as a mean porosity value is required for the whole thickness of the crust, the general observation is that the fracture porosity decreases very rapidly away from the crustal faults. Very near crustal fault (San Gabriel site), maximum values, that may be attributed to a single earthquake event (according to isotope results), reach about 10%. Much lower mean fracture porosity values are found some tens or hundreds meters away from the faults (1–2% of cumulative fracture elongation in the Little Pine shales). Consequently, we made the simplified assumption, that after each earthquake, the mean porosity profile through the whole crustal section, decreases exponentially away from the fault (Figure 9c, $t = 0$).

[43] Two main relations are used, expressing fluid mass conservation $\partial(\rho\phi)/\partial t + \mathrm{div}(\rho V) = 0$ and Darcy's law $V = \mathbf{K}(\nabla P + \rho g)$, where ρ is the density of the fluid, ϕ is the connected mean porosity of the rock, V is the Darcy flow rate (fluid particle velocity times porosity), $\mathbf{K}$ is the permeability tensor, P is the total pore pressure and g is the gravity. ∇ and div represent the gradient and divergence operators. Let us define the approximations in the model. First, during the evolution, we consider that the density $\rho = \rho' + \rho_m$ will evolve in time of an amount ρ' around its local mean value ρ_m, and finally, we rewrite the fluid mass conservation by neglecting the terms ρ' compared to ρ_m. For simplicity, ρ_m is taken constant and homogeneous in the crust. Second, we consider that the total pore pressure P can be decomposed as $P = p + P_{\mathrm{hydro}}$ such that P_{hydro} is the hydrostatic pressure verifying $\nabla P_{\mathrm{hydro}} + \rho_m g = 0$. Third, we consider that the principal directions of the permeability tensor $\mathbf{K}$ are the axes of the fault frame x, z, which means that the anisotropy of the permeability takes the natural direction of the fault. This last assumption seems reasonable if the fault has a constant straight and vertical shape. By applying these three simplifications, we rewrite the fluid mass conservation and Darcy's law in the following simplified form:

$$\phi\partial\rho'/\partial t + \rho_m\partial\phi/\partial t + \partial(\rho_m V_x)/\partial x + \partial(\rho_m V_z)/\partial z = 0 \qquad (9)$$

$$V_x = -K_x\partial p/\partial x \qquad V_z = -K_z\partial p/\partial z, \qquad (10)$$

where V_x and V_z are the components of the Darcy flow rate and K_z and K_x are the permeability coefficients parallel to z and x, respectively. The two permeabilities K_z and K_x are chosen to express a high anisotropy with a ratio $K_z/K_x = 100$. This ratio is chosen to allow a reasonable fluid transfer across the fault zone. Field observations suggest an even stronger anisotropy [*Rice*, 1992]. It is assumed that the variation of the density of the fluid ρ' is only due to the variation of the fluid pressure p. This dependence is simply expressed with a compressibility factor $C_f = 1/\rho_m(\partial\rho'/\partial \mathrm{p})$ taken as a constant. In consequence we have a new expression of $\partial\rho'/\partial t = \rho_m C_f \partial p/\partial t$. It is also assumed that the

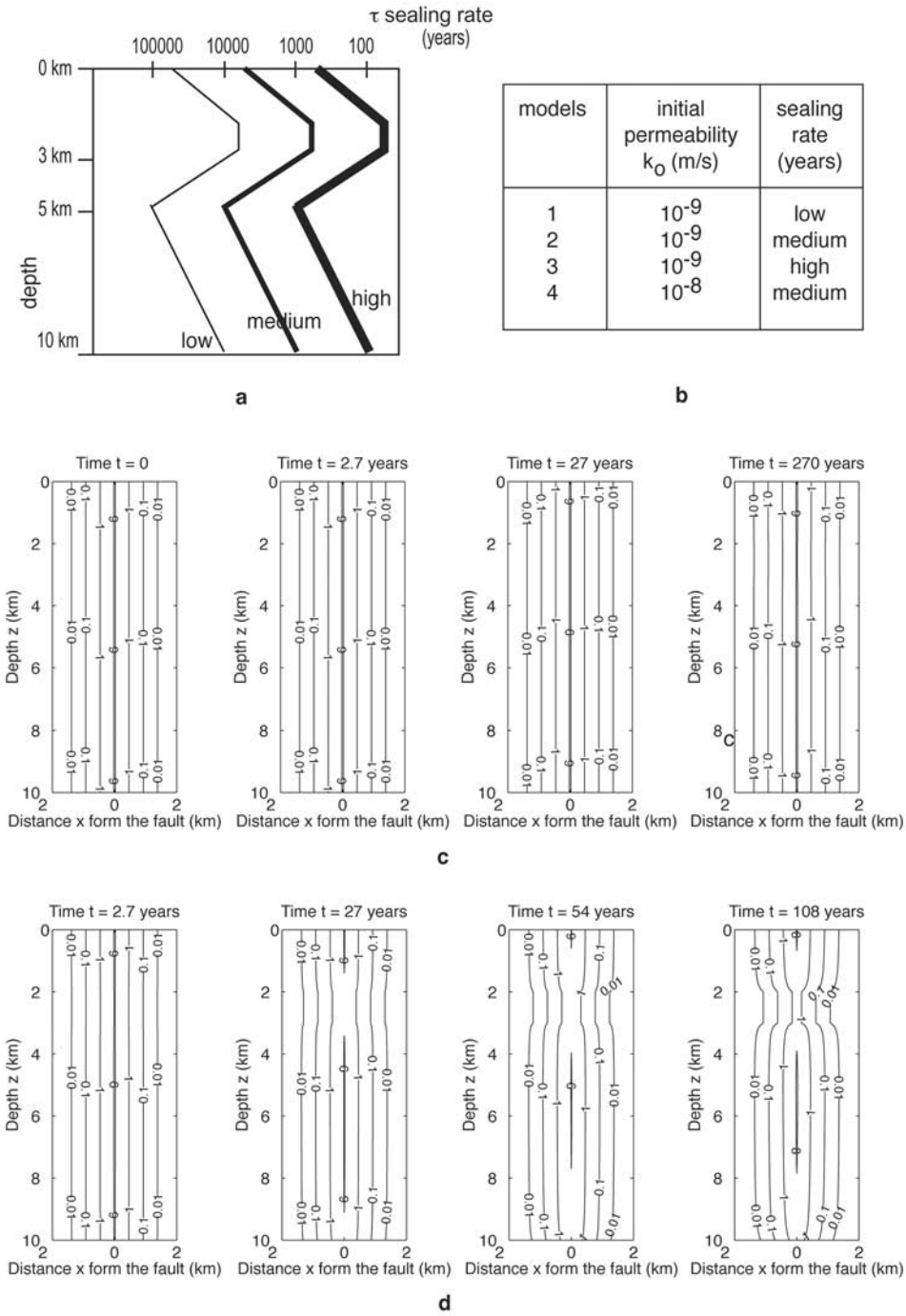

models	initial permeability k_O (m/s)	sealing rate (years)
1	10^{-9}	low
2	10^{-9}	medium
3	10^{-9}	high
4	10^{-8}	medium

Figure 9. Modeling of mass transfer and change in pressure along active faults. (a) Synthetic variation in crack sealing rate with depth integrating two superimposed calcite-rich and quartz-rich levels: crack sealing is modeled with pure calcite between 0 and 3 km, pure quartz between 5 and 10 km and intermediate behavior between 3 and 5 km. Crack sealing is expressed as the τ values (time require in order to divide the initial porosity by 2.72). Three sets of crack sealing values are derived from this section: low, medium and high sealing rate profiles. (b) Table of values of the main modeling parameters: initial permeability k_0 and sealing rate. The initial porosity along the fault is 10% (Figures 9c, 10, and 11) or 1% (Figures 12 and 13). (c) and (d) Evolution of the porosity values with time (t), through crustal cross section perpendicular to the fault (located at $x = 0$); Figure 9c for $t = 0$ gives the initial porosity profile; evolution in Figure 9c is obtained with the lowest sealing rate (model 1, Figure 9b), evolution in Figure 9d is obtained with the highest sealing rate (model 3, Figure 9b).

porosity equals $\phi = \phi_m + \phi'$ will vary at two independent amplitude scales. The ϕ_m is the mean local porosity that varies strongly and heterogeneously in time because of the kinetics of the crack sealing process (see below). The ϕ' is the smaller variation of the porosity due to the fluid pressure variation. Therefore we write $\partial\phi/\partial t = \partial\phi_m/\partial t + \partial\phi'/\partial p \partial p/\partial t$. The pore pressure dependence of ϕ' is defined by a simple matrix compressibility factor $C_m = 1/\phi_m(\partial\phi'/\partial p)$. Rigorously, by following the Biot theory of poroelasticity, reformulated later by [*Rice and Cleary*, 1976], the pore pressure should also depend on the variations of the state of total stress or the state of strain of the crust. For simplicity, we will consider that the state of total stress of the crust will not change significantly during the pressurization. This rough approximation is the main limit of the model. Indeed it does not consider the interaction involved by the poroelastic theory, which is out of the scope of this paper. Therefore, by considering, in first approximation, that the variations of the state of total stress of the crust are small, we have $C_m = C_d\,[(C_d - C_s)/(\phi_m C_s) - 1]$, where C_s is the compressibility of the pure solid part and C_d is the compressibility of the skeleton, i.e., the dried solid part containing the pores. During the simulation, the mean porosity ϕ_m will decrease significantly in time, due to the pressure solution, but at the same time C_d tends to reach C_s. This is why we assume that the compressibility of the matrix C_m can reasonably be taken as a constant. We can now combine equations (9) and (10) with the upper assumptions. In addition, we neglect the remaining second order terms involving the product $\phi'\rho'$ to obtain the following relation for the pore overpressure p:

$$\phi_m C(\partial p/\partial t) + (\partial\phi_m/\partial t) = (\partial/\partial x + \partial/\partial z)(K_x \partial p/\partial x + K_z \partial p/\partial z). \tag{11}$$

In expression (11), $C = (C_f + C_m)$ expresses the mean matrix-fluid compressibility and $\phi_m C$ represents the pressure storativity. This storativity will naturally decrease with the porosity ϕ_m because of the crack sealing process. Simplified expression (11) is a linear diffusion equation with time and space dependent coefficients and a forcing term $\partial\phi_m/\partial t$. The porosity ϕ is expressed as a function of space and time following natural observations (Figure 9c, $t = 0$) and crack sealing modeling (Figures 8b and 8c), respectively:

$$\phi_m(x,z,t) = \phi_0 e^{-x/L} e^{-t/\tau(z)}$$

and, consequently,

$$\partial\phi_m/\partial t(x,z,t) = -\phi_0 e^{-x/L} e^{-t/\tau(z)}/\tau(z). \tag{12}$$

L is the characteristic distance for the exponential decrease of the porosity after each earthquake (distance for which the maximum porosity ϕ_0 along the fault is divided by 2.72). The $\tau(z)$ is the characteristic time of the sealing process (time during which the porosity is divided by 2.72). The shape of $\tau(z)$ as been derived from a stratified crust with different rates of compaction using the results of the crack sealing modeling (see Figure 9a). In the upper crust, we assume the predominance of the calcite rate of crack sealing at low temperature and pressure while in the deeper crust we assume the predominance of the rate of crack sealing of the quartzite at higher temperature and pressure [*Renard et al.*, 2000]. The depth of transition between these two end-member cases is chosen to be at 3 km (Figure 9).

[44] Following *Lockner and Evans* [1995], the time dependence between porosity and permeability during sealing processes may be expressed as

$$k(t) \approx \phi_m(t)^3. \tag{13}$$

This leads to the following relation for the permeability:

$$\begin{aligned} K_x(x,z,t) &= (k_0/\rho_m g) e^{-x/L} e^{-3t/\tau(z)} \\ K_z(x,z,t) &= 100(k_0/\rho_m g) e^{-x/L} e^{-3t/\tau(z)}, \end{aligned} \tag{14}$$

where k_0 is the "kinematic" permeability, having the dimension of a velocity. The factor 3 is not reported on the spatial variation since we do not consider that the initial permeabilities K_x (x, z,0) and K_z (x, z,0) can be easily related to the initial porosity ϕ_m (x,z,0). We consider that only their rate of variation in time is relevant. Finally, the total fluid pressure must not exceed the lithostatic pressure. This may be written

$$p(x,y,t) < P_{\text{litho}} - P_{\text{hydro}} \propto -g(\rho_{\text{litho}} - \rho_m)z, \tag{15}$$

where g is the mean gravity in the crust, oriented along z. The combination of equations (11), (12), and (14) is still a linear approach, even nonhomogeneous, but the addition of condition (15) leads to a nonlinear problem. Condition (15) corresponds to a cutoff due to hydraulic fracturing of the crust. It is not sufficient to describe the system completely because as soon as condition (15) is reached, the permeability should increase brutally, making an important local fluid flow and a release of pore pressure. In our model, we consider a monotonic evolution of the pore pressure, that is when a region reaches the criterion (15) at time t_{litho}, it will not unload later, i.e., $p(x,y,t > t_{\text{litho}}) = P_{\text{litho}} - P_{\text{hydro}}$. Therefore the boundary of the region that has reached the lithostatic pressure is a moving pressure-imposed boundary and the fluid flow inside this region is still evaluated with equation (10).

[45] The calculation was based on the following boundary conditions: at $z = 0$ (surface), free surface, i.e., $p = 0$; at $x = 0$ (within the fault), symmetry then null flow, i.e., $\partial p/\partial x = 0$; at $x = 2$ km (far from fault), hydrostatic pressure, i.e., $p = 0$; and at $z = -h = -10$ km (transition between brittle and plastic behavior), imposed pressure zone scaled with the fault zone, i.e., $p = gh\,(\rho_{\text{litho}} - \rho_m)\,e^{-x/L}$. Just after an earthquake, the initial condition at $t = 0$ is $p = 0$ (and consequently $\phi' = 0$ and $\rho' = 0$).

[46] Several calculations have been performed with an explicit finite difference method. The modeling main parameter values are given in Figure 9b. The following reasonable values are used for all the models: $g = 10$ m s^{-2}, $\rho_{\text{litho}} = 2800$ kg m^{-3}, $\rho_m = 880$ kg m^{-3}, $\phi_0 = 10\%$ or 1%, $L = 100$ m, and $1/C = 1$ GPa; ϕ_0 is a maximum porosity value along the fault, the initial porosity profile shows an exponential decrease away from the fault (Figure 9c, $t = 0$).

Various calculations have been done with two values of k_0, i.e., $k_0 = 10^{-9}$ m s^{-1} and 10^{-8} m s^{-1}. By taking a fluid viscosity of $\eta = 1.5 \times 10^{-4}$ Pa s (at 160°C, 5 km), $k_0 = 10^{-9}$ m s^{-1} corresponds to a geometric permeability $k_0\eta/\rho_m g = 1.7 \times 10^{-17}$ m^2. This quite high value corresponds to the one at the center of the fault at the beginning of the process, i.e., in the most damaged zone after an earthquake. However, following equation (14), the permeability decreases strongly far from the fault plane and also in time because of crack sealing. For the kinetics of crack sealing, a simplified variation with depth is used, assuming that the rate of sealing is controlled by calcite between 0 and 3 km, by quartz between 5 and 10 km, and by an intermediate behavior between 3 and 5 km (see Figure 9a). Because of the uncertainty on the parameters of the calculation the same profile has been used with three different orders of magnitude for the τ values (i, j, k) with the following minimum and maximum values (Figure 9a): (1) = 10,000 > τ_i > 700; (2) = 1000 > τ_j > 70, and (3) = 100,000 > τ_k > 7000 years. The medium (τ_j) values correspond to spacing between fractures, which is of the order of magnitude of 100 μm (with crack width of 6 μm). Shifting the τ values by 1 order of magnitude higher (τ_k) or lower (τ_i) corresponds to spacing of 200 or 50 μm, respectively (with crack widths of 12 or 3 μm, respectively). From the observations of natural crack sealing, a mean spacing of 100 to 200 μm seems realistic (Figures 4, 5, and 6). The sealing rates used here were also chosen as fast as realistic in order to be able to run the calculation for an acceptable time.

5.2. Results and Discussion

[47] Results of the modeling are given in Figures 9, 10, 11, 12, and 13. Figures 9c and 9d show the evolution of the porosity profile with time through a vertical cross section of the crust, with initial porosity of 10% along the fault surface. The effect of the crack sealing rate is clear between its lowest value (Figure 9c, almost no change even after 270 years) and its highest value (Figure 9d, change after some tens years). Figure 10 shows the pressure distribution in cross sections perpendicular to the fault. Figure 11 shows the distribution of upward flow rates both in time and space (same cross sections as for pressure distribution). The effects of the two competing processes (influx from depth and sealing rate around the fault) are observed in both Figures 10 and 11. Just after an earthquake, overpressure always develops at the bottom of the fault because of the inflow of fluid from depth. All the models show this effect (Figure 10), leading to a very localized high pressure zone (up to lithostatic values) that develop a short time after an earthquake (years). With the lowest sealing rates (Figure 10a) overpressure slowly extends to the entire fault zone. After several hundred years, normalized overpressure, $O_{vp} = p/(P_{\text{litho}} - P_{\text{hydro}})$, with $0 < O_{vp} < 1$, reaches values of about 0.6 in the median part of the fault zone. The calculation could not be run for more time, but it could take thousand years or more to develop lithostatic pressure all along the fault. In all the cases also (Figure 10), another overpressure zone develops in the upper part of the seismic zone (between 2 and 5 km depth) due to the fast sealing rate of calcite. However, the development of such an overpressure zone is strongly dependent on the kinetics of crack sealing. This may be seen when comparing the pressure distribution obtained for different models with low, medium, and high sealing rate in Figures 10a, 10b, and 10c, respectively. Such an overpressure in the upper part of the seismic crust intensely develops after only several tens years with the highest sealing rate (Figure 10c). Local overpressure also develops at 3 km depth with medium sealing rate, but only after several hundred years (Figure 10b). Finally, very tenuous overpressure is noted in the same zone after several hundred years with the slowest sealing rate (Figure 10a). With high sealing rate values, the effect is so strong that after hundred years, it prevents the fluid to flow out of the crust toward the Earth's surface (Figure 10c). This effect appears even more clearly in Figure 11, which shows the distribution of flow rates through the Earth's surface, both in space and time. Evolution of upward flow rates with time confirms the crucial effect of the kinetics of crack sealing when comparing Figure 11a (low sealing rates) and Figure 11c (fast sealing rates): fast sealing rate drastically decreases the upward fluid flow rate after about a hundred years. With high sealing rate, the high flow rate during the first hundred years is related to both inflow from depth and upward fluid expulsion due to the fast compaction.

[48] The effect of the initial permeability coefficient appears when comparing the modeling with the highest ($k_0 = 10^{-8}$ m s^{-1}, Figure 10d) and the lowest permeability ($k_0 = 10^{-9}$ m s^{-1}, Figure 10d). Increase in permeability value facilitates the flow-through process along the fault and so amplifies the development of overpressure at the bottom

Figure 10. (opposite) Fluid transfer modeling along active crustal faults when integrating pressure solution crack sealing processes in parallel with inflow of deep lower crust fluids (see Figure 9b); evolution of normalized fluid overpressure $O_{vp} = p/(P_{\text{litho}} - P_{\text{hydro}}) = (P - P_{\text{hydro}})/(P_{\text{litho}} - P_{\text{hydro}})$. The initial porosity along the fault surface is 10%. Time-dependent variation is from left to right (from 2.7 to 270 years). The τ values are the time duration requires in order to divide the initial porosity by 2.72 (see Figure 9a). (a) Model 1, initial permeability $k_0 = 10^{-9}$ m s^{-1}, low sealing rate; overpressure rapidly increases at depth (zone with O_{vp} values = 0.9) then very slowly extends to the entire fault zone (O_{vp} values reaching 0.6 after several hundred years). (b) Model 2, initial permeability $k_0 = 10^{-9}$ m s^{-1}, medium sealing rate; same fast localized overpressure development at depth (red zone) slowly extending to the whole fault. However, medium sealing rate allows localized overpressure development in the upper part of the seismic crust (270 years). (c) Model 3, initial permeability $k_0 = 10^{-9}$ m s^{-1}, high sealing rate; same fast localized overpressure development at depth (red zone). However, high sealing rate rapidly develops localized overpressure in the upper part of the seismic crust and prevents the outflow of the fluid (before 108 years). (d) Model 4, initial permeability $k_0 = 10^{-8}$ m s^{-1}, medium sealing rate; same fast localized overpressure development at depth (red zone) rapidly extending to the whole fault after some years (2.7 years), contrary to model 2. However, even with the effect of medium sealing rate values, localized overpressure finally develops in the upper part of the seismic crust as in model 2 (270 years).

of the seismic crust and progressively through the faults. This effect of the initial permeability is especially efficient when the sealing rate is low. In this case, change of 1 order of magnitude of the permeability values leads change of 1 order of magnitude of the flow rate values. However, with high or medium sealing rate the initial permeability effect is more complex. For example, in the case of medium sealing rate, when comparing Figures 10b and 10d, the model with the highest permeability develops the highest overpressure during the first tens of years; however, after several hundred years the effect of different initial permeability is not so significant.

[49] The effect of the initial porosity values is shown by comparing Figure 10 (initial porosity $\phi_0 = 10\%$) and Figure 12 (initial porosity $\phi_0 = 1\%$), but we still take the same initial permeability ($k_0 = 10^{-9}$ m s^{-1}). Remembering that the timescale of the process is linked to the storativity $\phi_m C$ and therefore to the porosity, we remark that a lower value of the initial porosity (1%) leads to a fastest increase of fluid pressure during the first years. However, the difference due to the initial porosity progressively diminish with time and after several hundred years the pressure distribution is almost the same for initial porosity of 10% or 1%. At larger times, the flux coming from depth dominates the evolution.

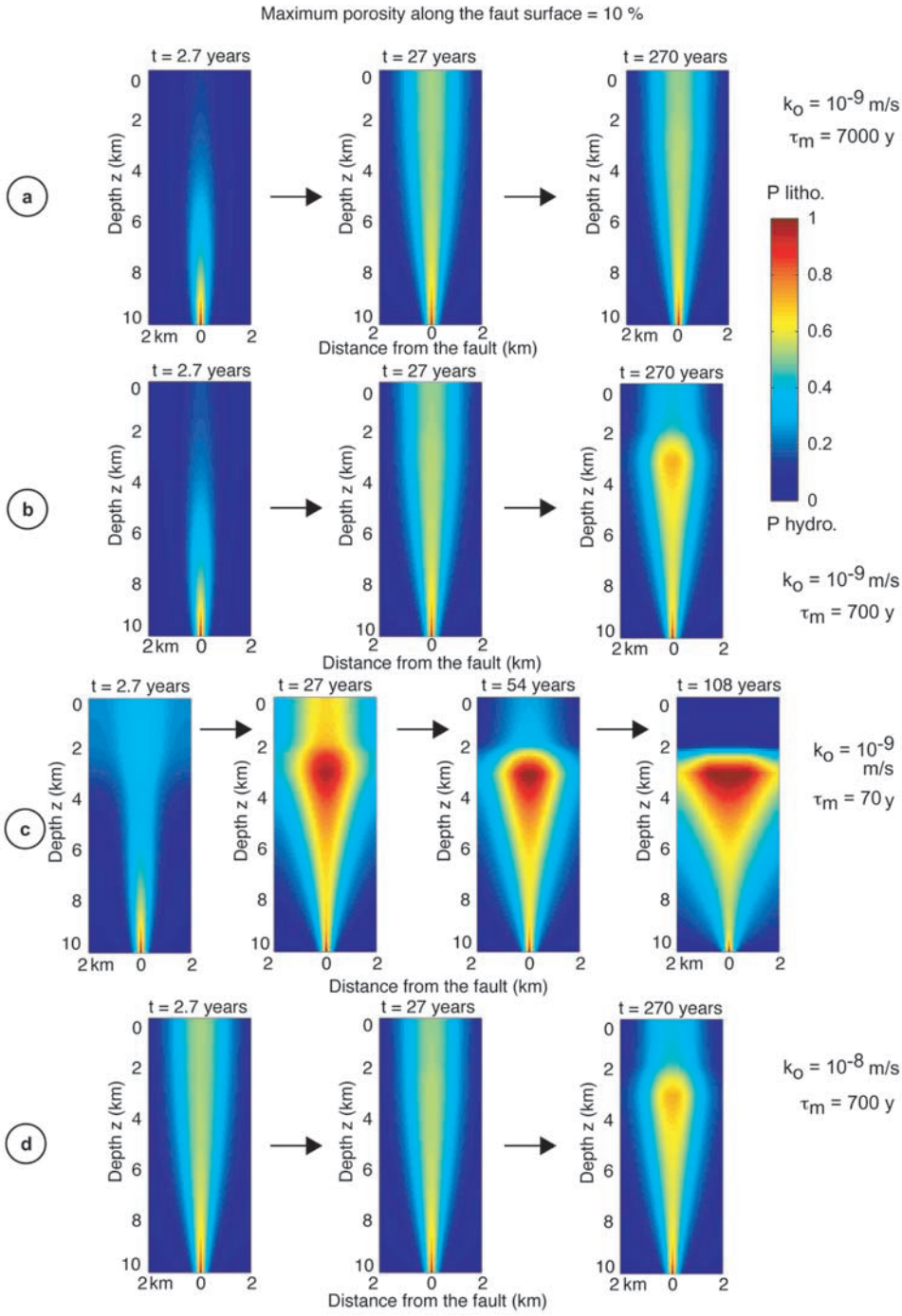

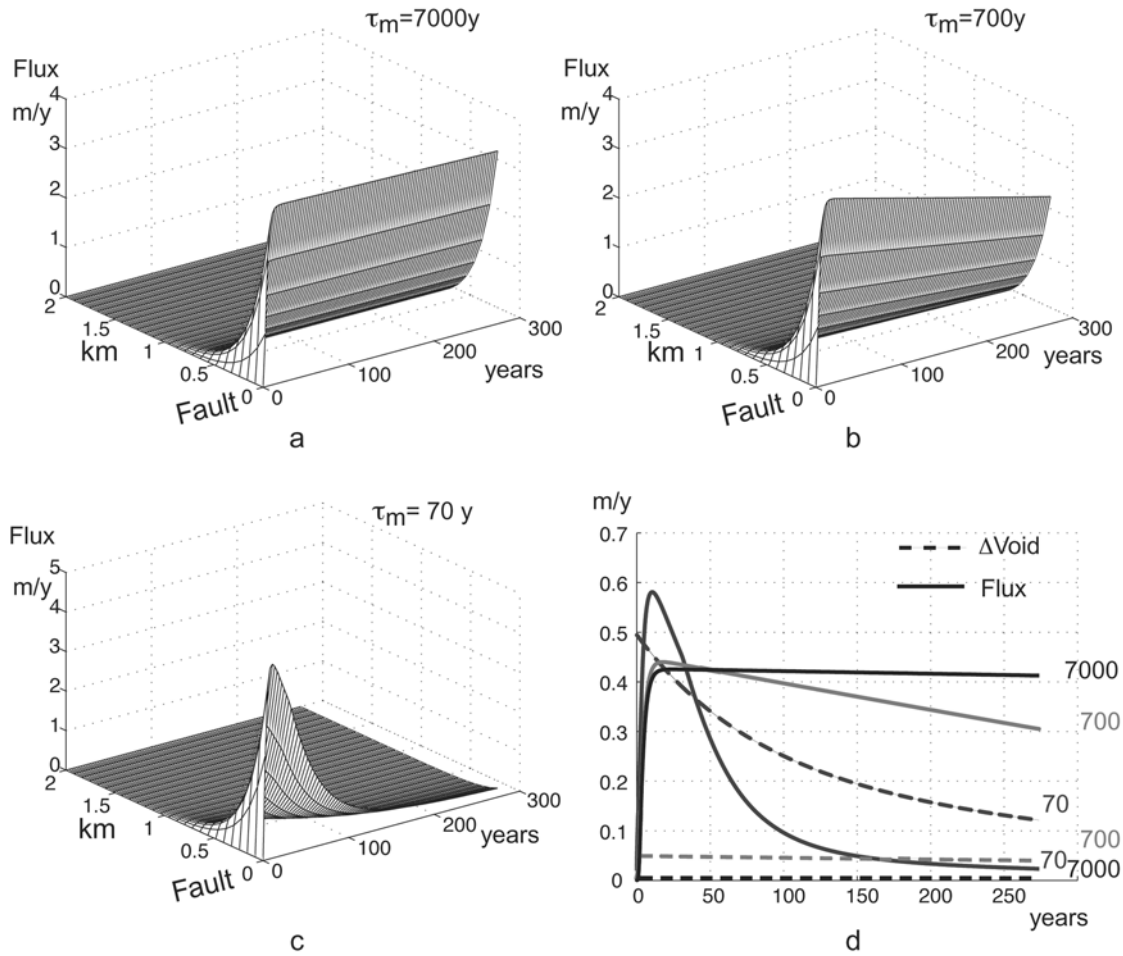

Figure 11. Fluid transfer modeling along active crustal faults when integrating pressure solution crack sealing processes in parallel with inflow of deep lower crust fluids (see Figure 9); evolution of the upward fluid flow rates (m yr^{-1}) both in space (same vertical cross sections as in Figure 10, perpendicular to the fault plane) and time (2.7–270 years). The initial porosity along the fault surface is 10%. The τ values are the time duration required in order to divide the initial porosity by 2.72 (see Figure 9a). (a) Model 1, initial permeability $k_0 = 10^{-9}$ m s^{-1}, low sealing rate; τ_m = 7000 years. (b) Model 2, initial permeability $k_0 = 10^{-9}$ m s^{-1}, medium sealing rate; τ_m = 700 years. (c) model 3, initial permeability $k_0 = 10^{-9}$ m s^{-1}, high sealing rate; τ_m = 70 years. (d) For the three models; solid lines, evolution of the mean upward flow rate (m yr^{-1}) integrated along a half-space of 2 km (1 m width); dashed lines, evolution of the mean voids volume change rate (m yr^{-1}) integrated along a half-space of 2 km (1 m width).

[50] On Figures 11d and 13d (for initial porosity of 10% and 1%, respectively) we plot the mean flow rates calculated by integrating the upward surface flow rate along the cross section (axe X) and by dividing it by the thickness of the model (2 km). With initial porosity at 10% along the fault surface, mean values of 0.42, 0.37, and 0.14 m yr^{-1} are found respectively for low, medium and high sealing rates, over duration of 270 years and for half-space of 2 km around the fault. These values are almost divided by 2 with 1% of initial porosity along the fault surface. These mean upward flow rates may be compared to the ones estimated by [*Kennedy et al.*, 1997] from helium isotopic study. Kennedy et al. found that present fluids associated with the San Andreas fault system show evidence of mantle $^3He/^4He$ ratios. As during the flow-through process, high fluid ratios from depth are diluted with radiogenic ^4He produced in the crust, they were able to estimate the minimum flow rates, which control the dilution. Flow rates of 3 to 10 mm yr^{-1} were estimated, which are also minimum values since constant permanent flow was assumed. Our values ranked at least 1 order of magnitude above these minimum values. However, our values are related to a narrow flow-through zone (2 km). Heterogeneous fluid flow around the faults may complicate the comparison between the two calculations. Fitting the two sets of results could have been possible, however, taking into account the approximations on both calculations this was not done.

[51] In our calculation, the sealing rate is derived from pressure solution crack-sealing modeling. However, one may argue that deposition from flow-through saturated fluids may contribute to the sealing of the veins by the effect of both decreasing temperature and pressure. To test this contribution, which has not been integrated in our

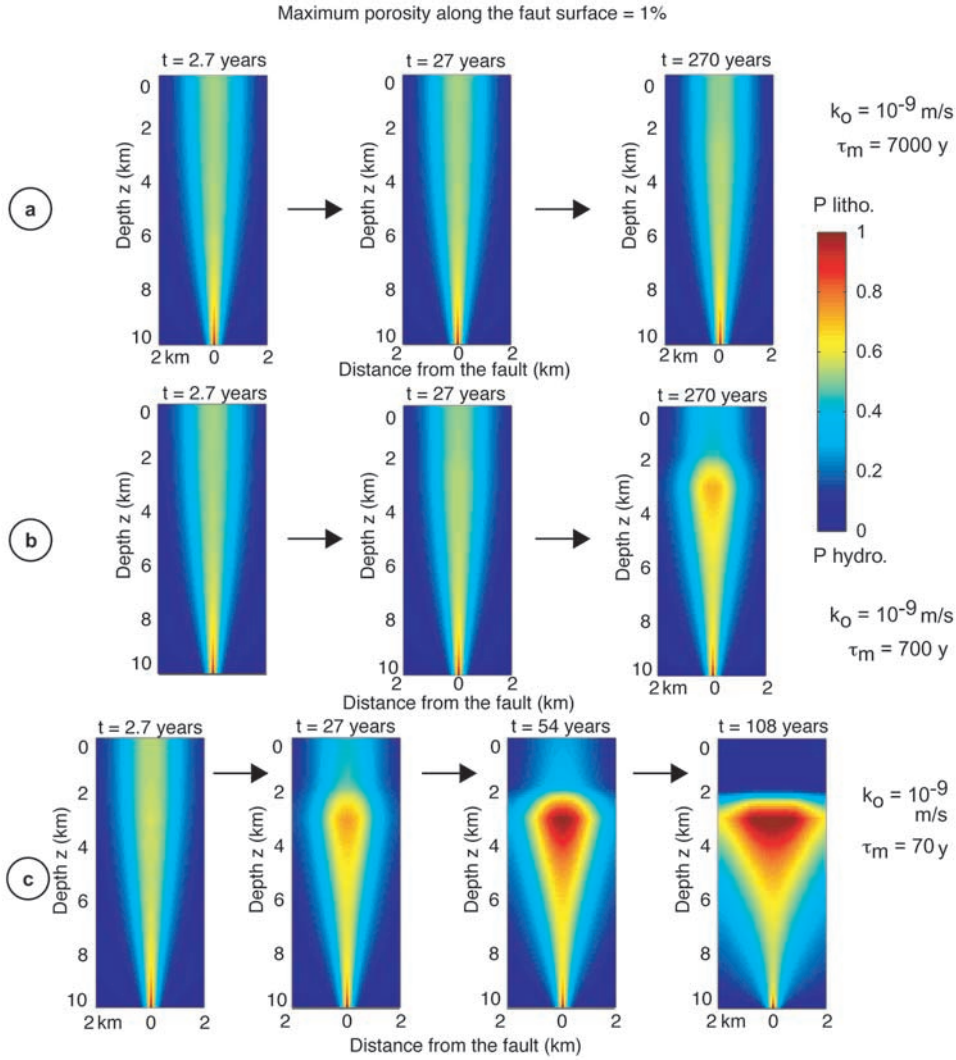

Figure 12. Fluid transfer modeling along active crustal faults when integrating pressure solution crack sealing processes in parallel with inflow of deep lower crust fluids (see Figure 9b); evolution of normalized fluid overpressure $O_{vp} = p/(P_{\text{litho}} - P_{\text{hydro}}) = (P - P_{\text{hydro}})/(P_{\text{litho}} - P_{\text{hydro}})$. The initial porosity along the fault surface is 1%. Time-dependent variation from left to right (from 2.7 to 270 years). The τ values are the time duration requires in order to divide the initial porosity by 2.72 (see Figure 9a). (a) Model 1, initial permeability $k_0 = 10^{-9}$ m s^{-1}, low sealing rate; overpressure rapidly increases at depth (zone with O_{vp} values of 0.9) and through the entire fault (faster than with 10% initial porosity, Figure 10), O_{vp} values reaching 0.6 after several years. (b) Model 2, initial permeability $k_0 = 10^{-9}$ m s^{-1}, medium sealing rate; same fast localized overpressure development at depth (red zone) and through the entire fault (faster than with 10% porosity) (O_{vp} values reaching 0.6 after several years). However, the medium sealing rate allows localized overpressure development in the upper part of the seismic crust (270 years). (c) Model 3, initial permeability $k_0 = 10^{-9}$ m s^{-1}, high sealing rate; same fast localized overpressure development at depth (red zone), high sealing rate rapidly develops localized overpressure in the upper part of the seismic crust and prevents the outflow of the fluid (before 108 years) as with 10% initial porosity (see Figure 10).

calculation for simplicity, it is possible to compare the volume of flow through fluid versus the volume of deposition. The first one is derived from the mean upward flow (see above): 113, 101, and 39 m^3 m^{-2}, over 270 years and along a half-space of 2 km from the fault for low, medium, and high sealing rates, respectively. As a broad approximation, the deposed volume may be the difference between the volume of the voids at the beginning and at the end of the modeling. The voids volume change rate is given in Figures 11d and 13d (dashed lines) for 10% and 1% initial porosity, respectively. Integrating these values, both in space and in time, gives a broad estimation of the sealed volume: 1.3, 12, and 65 m^3 m^{-2}, for 10% initial porosity, this over 270 years and along a half-space of 2 km from the fault for low, medium, and high sealing rates, respectively. The sealed volume is 10 times below with 1% as initial porosity. Even

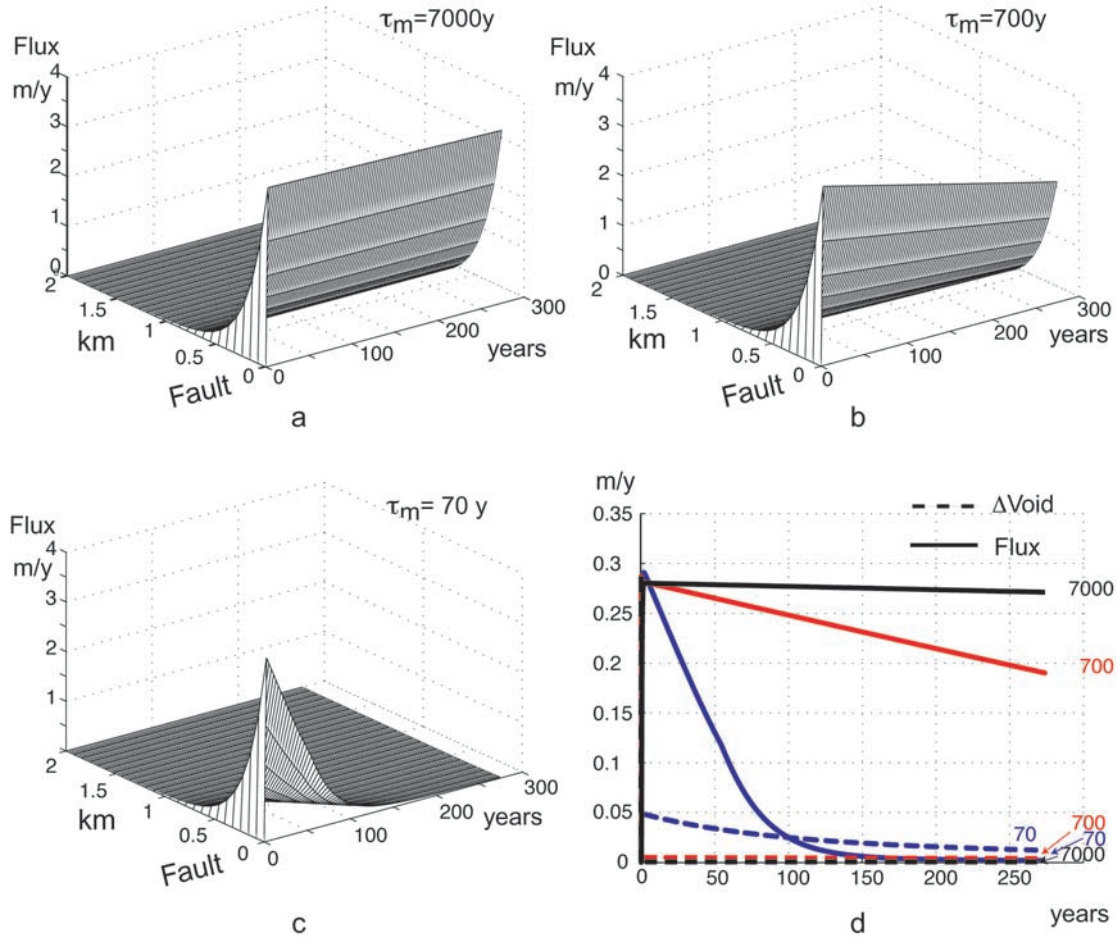

Figure 13. Fluid transfer modeling along active crustal faults when integrating pressure solution crack sealing processes in parallel with inflow of deep lower crust fluids (see Figure 9); evolution of the upward fluid flow rates (m yr^{-1}) both in space (same vertical cross sections as in Figure 12, perpendicular to the fault plane) and time (2.7–270 years). The initial porosity along the fault surface is 1%. The τ values are the time duration required in order to divide the initial porosity by 2.72. (a) Model 1, initial permeability $k_0 = 10^{-9}$ m s^{-1}, low sealing rate; $\tau_m = 7000$ years. (b) Model 2, initial permeability $k_0 = 10^{-9}$ m s^{-1}, medium sealing rate; $\tau_m = 700$ years. (c) Model 3, initial permeability $k_0 = 10^{-9}$ m s^{-1}, high sealing rate; $\tau_m = 70$ years. (d) For the three models; solid lines, evolution of the mean upward flow rate (m yr^{-1}) integrated along a half-space of 2 km (1 m width); dashed lines, evolution of the mean voids volume change rate (m yr^{-1}) integrated along a half-space of 2 km (1 m width).

for the lowest sealing rates, the highest calculated ratio between fluid volume and deposition volume is lower (10^2–10^3) than the ratio required for example between aqueous solution and quartz deposition when considering that all the sealing minerals derived from deep fluids (3 10^4) [*Fyfe et al.*, 1978]. Moreover, deep fluids are not necessarily aqueous solution and only part of the total dissolved species would precipitate. So only a small part of the porosity could be sealed by the effect of external fluids even with low sealing rates. Consequently, the modeling shows that significant change of porosity and permeability may occur without large fluid flow volume. However, evidence of inflow from depth was found anyway from isotope studies [*Pili et al.*, 1998], so the role of the deep fluids may be mainly to wet the connected fractured network around the fault after each earthquake. Then stress- driven local mass transfer is activated (Figures 3, 4, 5, and 6) and develops during interseismic period largely contributing to the sealing of the rocks by residual postseismic stress relaxing around the fault.

[52] The development of such high-pressure zones within the upper part of the seismic crust is strongly dependent on the presence of calcite. If calcite is not available to seal the cracks, then the upper zone of high pore pressure never develops. Observations in the three different Californian sites show that above 2 km within the crust, most of the sealing minerals are carbonates especially calcite. The same observation is made in other active faults such as in the Nojima fault, Japan [*Boullier et al.*, 2000]. It must be noted that using high sealing rates helps to show the development of the high fluid pressure zone in the upper part of the seismic crust during a limited time of calculation. However, even with the slowest sealing rates (Figures 10a, 10b, 12a, and 12b), such high fluid pressure

develops in the upper part of the seismic crust after several hundred years. Consequently, the effect of preventing outflow toward the Earth's surface must develop as well as in Figures 10c–12c but with very longer time (thousand years or more).

[53] This calculation is pertinent for faults affecting the entire brittle crust (San Andreas type, see cross section in Figure 2). Because of the complexity of the earthquake process, this does not give the recurrent time of each rupture on the same fault segment, but it gives some characteristic time involved in the seismic cycle. Progressive stress loading due to geodynamic processes, overpressure evolution, and complex interaction between faults play a major role in earthquake development. However, as overpressure reduces the strength of the faults, the zone of high fluid pressure, developing during interseismic cycle, may correspond to the zone of nucleation of the next earthquake. The two effects that control the overpressure process (crack sealing and inflow from depth) compete to impose overpressure distribution. High fluid pressure is shown here to develop in the seismic crust either in the upper part or in the lower part depending on both the sealing rate vertical profile and the initial permeability. This may explain, at least partially, why some earthquakes initiate in the upper part of the crust and propagate downward, whereas others initiate in the lower part of the upper crust and propagate upward.

6. Conclusions

[54] 1. Observations of natural deformation in the country rocks around active faults in California (San Gabriel, Little Pine, and Melones faults) reveal that fractures developing during earthquakes are progressively sealed during the interseismic period. Crack sealing mostly occurs with an input of matter locally derived from pressure solution cleavage and stylolites. The progressive compaction of the gouge that also occurs during interseismic period is partly controlled by pressure solution.

[55] 2. Pressure solution rates depend on the nature of the limiting processes: kinetics of reaction or diffusive mass transfer. Fast free-face reactions occur after earthquakes in Californian faults (self-healing processes, temperature-decrease driven reactions). However, decrease in porosity is controlled mainly by very slow diffusion-limited stress-driven processes that relaxes postseismic stress.

[56] 3. Coupled inflow of supersaturated fluids from depth is attested both by stable isotope studies and by observations of typical mineral deposits in the gouge of the Californian faults. This inflow contributes to the decrease in porosity during the interseismic period, mainly in the gouge. However, it has minor effects on the sealing of nearby fractured country rocks.

[57] 4. Postseismic pressure solution processes are very dependent on the microfracture network created by earthquakes. When integrating both crack sealing and gouge compaction in pressure solution modeling, porosity versus time exponential relations are derived from Californian fault observations and laboratory experiments.

[58] 5. Postseismic strain rate versus time exponential relations are also derived from pressure solution crack seal modeling and such relations fitted well with the recording of significant postseismic ductile deformation in the upper crust.

[59] 6. Fluid pressure variations during the interseismic period were numerically modeled for typical Californian crustal structure and related strike-slip faults. This was done by integrating both flow-through external fluids and progressive modeled decrease in porosity, and related permeability, around the fault by pressure solution.

[60] 7. Results of the modeling give characteristic times for the change of fluid pressures during interseismic periods and thus for the change in mechanical strength of the fault. The modeling shows the drastic effect of the kinetics of crack sealing within and around the fault, not only on the rate of increase of fluid pressure but, more surprisingly, on the distribution of the fluid pressure. Overpressure distribution is dependent on the values of both parameters: the initial permeability and its rate of change with time by crack sealing. (1) A zone of very localized high-pressure always develops at depth due to the inflow of deep fluids, its development is fast (years) and is controlled by the initial permeability of the fault. (2) Because of the fast sealing effect of calcite, another much larger zone of high pressure can develop in the upper part of the seismic crust if this mineral is present. Depending on the sealing rate, it could take between tens to several hundred years to develop such high-pressure zones. (3) Finally, orders of magnitude of thousand years or more are calculated for the recovery of lithostatic pressure all along a crustal fault after an earthquake that lowered the fluid pressure to a hydrostatic value.

[61] 8. Assuming that high fluid pressure locally reduces the strength of the fault and locates the rupture, earthquake nucleation and propagation may vary according to the effects of several parameters: initial permeability, crack sealing rate, nature and geometry of the damaged fault zone.

[62] 9. The modeling also gives an order of magnitude of the amount of external fluid associated with flow-through from depth. Such influxes are not found to be as high as presumably thought when considering that all the sealing minerals derived from deep fluids. Fluid inflow from depth wets the fault after each earthquake and crack sealing occurs during the interseismic period mostly by locally derived stress driven mass transfer.

[63] **Acknowledgments.** Studies in California were supported by the Southern California Earthquake Center and the Institute for Crustal Studies, UC Santa Barbara for the stays of one of us (J.P.G.). All computations presented in this paper were performed at the "Service Commun de Calcul Intensif de l'Observatoire de Grenoble" (SCCI). We thank C. Nicholson for helpful review, B. Patrick for scientific assistance, E. Pili for the review of the part dealing with isotope studies, and J.C. Crowell and R. Sibson for bringing one of us (J.P.G.) on the field to collect samples along the San Gabriel fault and in the Mother Lode valley, respectively.

References

Arthaud, F., and M. Mattauer, Exemples de stylolites d'origine tectonique dans le Languedoc, leur relation avec la tectonique cassante, *Bull. Soc. Géol. Fr.*, *11*, 738–744, 1969.

Bateman, P. C., and J. P. Eaton, Sierra Nevada batholith, *Sciences*, *158*, 1407–1417, 1967.

Bathurst, R. G. C., Diagenetically enhanced bedding in argillaceous platform limestones: Stratified cementation and selective compaction, *Sedimentology*, *34*, 749–778, 1987.

Bernard, D., J. P. Gratier, and A. Pêcher, Application de la microthermométrie des inclusions fluides des cristaux syncinématiques à un problème tectonique, *C. R. Sommaires Soc. Géol. Fr.*, *5*, 284–288, 1977.

Berry, F. A. F., High fluid potentiels in the California Coast Range and their tectonic significance, *Am. Assoc. Pet. Geol. Bull.*, *57*, 1219–1249, 1973.

Bohlke, J. K., and R. W. Kistler, Rb-Sr, K-Ar and stable isotope evidence for the ages and sources of fluid components of gold-bearing quartz veins in the northern Sierra Nevada Foothills metamorphic belt, California, *Econ. Geol.*, *81*, 296–322, 1986.

Boullier, A. M., and F. Robert, Palaeoseismic events recorded in Archaean gold-quartz vein networks, Val d'Or, Abitibi, Quebec, Canada, *J. Struct. Geol.*, *14*, 161–179, 1992.

Boullier, A. M., G. Michot, A. Pêcher, and O. Barrès, Diffusion and/or plastic deformation around fluid inclusions in synthetic quartz: New investigations, in *Fluid Movements-Element Transport and the Composition of the Deep Crust*, edited by D. Bridgwater, pp. 345–360, Kluwer Acad., Norwell, Mass., 1989.

Boullier, A. M., B. Ildefonse, J. P. Gratier, K. Fujimoto, T. Ohtani, and H. Ito, Deformation textures and mechanisms in the granodiorite from the Nojima Hirabayashi borehole, in *Proceedings of the International Workshop on the Nojima Fault Core and Borehole Data Analysis, Japan*, *U.S. Geol. Surv. Open File Rep., 00-129*, 111–117, 2000.

Brace, W. J., Pore pressure in geophysics, in *Flow and Fracture of Rocks, The Griggs Vol.*, *Geophys. Monogr. Ser.*, vol. 16, edited by H. C. Heard et al., pp. 265–273, AGU, Washington, D. C., 1972.

Brantley, S., B. Evans, S. H. Hickman, and D. A. Crerar, Healing of microcracks in quartz: implications for fluid flow, *Geology*, *18*, 136–139, 1990.

Brimhall, G. H., and D. A. Crerar, Ore fluids: Magmatic to supergene, in *Thermodynamic Modeling of Geological Materials: Minerals, Fluids and Melts*, *Rev. Mineral.*, vol. 17, edited by I. Carmichael and H. Eugster, pp. 235–254, Mineral. Soc. of Am., Washington, D. C., 1987.

Byerlee, J., Friction, overpressure and fault normal compression, *Geophys. Res. Lett.*, *17*, 2109–2112, 1990.

Cathles, L. M., An analysis of the cooling of intrusives by ground water convection which includes boiling, *Econ. Geol.*, *72*, 804–826, 1977.

Chester, F. M., J. P. Evans, and R. L. Biegel, Internal structure and weakening mechanisms of the San Andreas fault, *J. Geophys. Res.*, *98*, 771–786, 1993.

Cox, S. F., V. J. Wall, M. A. Etheridge, and T. F. Potter, Deformational and metamorphic processes in the formation of mesothermal vein-hosted gold deposits: Examples from the Lachlan fold belt in central Victoria, Australia, *Ore Geol. Rev.*, *6*, 391–423, 1991.

den Brok, S. B., Effect of microcracking on pressure-solution strain rate: The Gratz grain boundary model, *Geology*, *26*, 915–918, 1998.

Dewers, T., and P. Ortoleva, Geochemical self-organization, III, A mechano-chemical model of metamorphic differentiation, *Am. J. Sci.*, *290*, 473–521, 1990a.

Dewers, T., and P. Ortoleva, Interaction of reaction, mass transport, rock deformation during diagenesis: Mathematical modeling of intergranular pressure solution, stylolites and differential compaction cementation, in *Prediction of Reservoir Quality Through Chemical Modeling*, edited by I. D. Meshri and P. J. Ortoleva, *AAPG Mem.*, *49*, 147–160, 1990b.

Donnelan, A., and D. A. Lyzenga, GPS observations of fault afterslip and upper crustal deformation following the Northridge earthquake, *J. Geophys. Res.*, *103*, 21,285–21,297, 1998.

Elliot, D., The energy balance and deformation mechanisms of thrust sheets, *Philos. Trans. R. Soc. London, Ser. A*, *272*, 239–312, 1976.

Engelder, T., A natural example of the simultaneous operation of free-face dissolution and pressure solution, *Geochim. Cosmochim. Acta*, *46*, 69–74, 1982.

Etheridge, M. A., S. F. Cox, V. J. Wall, and R. H. Vernon, High fluid pressures during regional metamorphism and deformation: Implications for mass-transport and deformation mechanisms, *J. Geophys. Res.*, *89*, 4344–4358, 1984.

Evans, J. P., and F. M. Chester, Fluid-rock interaction in faults of the San Andreas system: inferences from the San Gabriel fault rock geochemistry, *J. Geophys. Res.*, *100*, 13,007–13,020, 1995.

Fisher, D. M., and S. L. Brantley, Models of quartz overgrowth and vein formation: Deformation and episodic fluid flow in an ancient subduction zone, *J. Geophys. Res.*, *97*, 20,043–20,061, 1992.

Fisher, D. M., S. L. Brantley, M. Everett, and J. Dzvonik, Cyclic fluid flow through a regionally extensive fracture network within the Kodiak accretionary prism, *J. Geophys. Res.*, *100*, 12,881–12,894, 1995.

Fyfe, W. S., N. J. Price, T. A. B., *Fluids in the Earth's Crust*, Elsevier Sci., New York, 1978.

Gibbs, J. W., On the equilibrium of heterogeneous substances. *Trans. Conn. Acad*, *3*, 108–248, 343–524, 1877.

Gratier, J. P., Estimation of volume change by comparing chemical analyses in heterogeneously deformed rocks, *J. Struct. Geol.*, *5*, 329–339, 1983.

Gratier, J. P., Pressure solution-deposition creep and associated tectonic differentiation in sedimentary rocks, in *Deformation of Sediments and Sedimentary Rocks*, edited by M. E. Jones and R. M. F. Preston, *Geol. Soc. London Spec. Publ.*, *29*, 25–38, 1987.

Gratier, J. P., Experimental pressure solution of halite by an indenter technique, *Geophys. Res. Lett.*, *20*, 1647–1650, 1993.

Gratier, J. P., and J. F. Gamond, Transition between seismic and aseismic deformation in the upper crust, in *Deformation Mechanisms, Rheology and Tectonics*, edited by R. J. Knipe and E. H. Rutter, *Geol. Soc. Spec. Publ.*, *54*, 461–473, 1990.

Gratier, J. P., and R. Guiguet, Experimental pressure solution-deposition on quartz grains: the crucial effect of the nature of the fluid, *J. Struct. Geol.*, *8*, 845–856, 1986.

Gratier, J. P., and L. Jenatton, Deformation by solution-deposition and reequilibration of fluid inclusions in crystals depending on temperature, internal pressure and stress, *J. Struct. Geol.*, *5*, 329–339, 1984.

Gratier, J. P., T. Hopps, C. Sorlien, and T. Wright, Recent crustal deformation in Southern California deduced from the restoration of folded and faulted strata, *J. Geophys. Res.*, *104*, 4887–4899, 1999a.

Gratier, J. P., F. Renard, and P. Labaume, How pressure-solution and fractures interact in the upper crust to make it behave in both a brittle and viscous manner, *J. Struct. Geol.*, *21*, 1189–1197, 1999b.

Gratz, A. J., Solution-transfer compaction of quartzites: Progress toward a rate law, *Geology*, *19*, 901–904, 1991.

Groshong, R. H., Low-temperature deformation mechanisms and their interpretation, *Geol. Soc. Am. Bull.*, *100*, 1329–1360, 1988.

Hadizadeh, J., and F. Foit, Feasibility of estimating cementation rates in brittle fault zone using Sr/Ca partition coefficients for sedimentary diagenesis, *J. Struct. Geol.*, *22*, 401–409, 2000.

Hedenquist, J. W., R. Reyes, S. F. Simmons, and S. Taguchi, The thermal and geochemical structures of geothermal and epithermal systems: A framework for interpreteting fluid inclusion data, *Eur. J. Mineral.*, *45*, 989–1015, 1992.

Hickman, S. H., and B. Evans, Experimental pressure solution in halite: The effect of grain/interphase boundary structure, *J. Geol. Soc. London*, *148*, 549–560, 1991.

Hubbert, M. K., and W. W. Rubey, Role of fluid pressure in the mechanics of overthrust faulting, part I, Mechanics of fluid-filled porous solids and its application to overthrust faulting, *Geol. Soc. Am. Bull.*, *70*, 115–166, 1959.

Ildefonse, J. P., Recherche sur le transport du silicium et du magnésium en conditions hydrothermales, Thèse d'Etat thesis, Univ. d'Orléans, Orléans, France, 1980.

Jennings, C. W., Fault activity map of California and adjacent areas with location and ages of recent volcanic eruptions, Calif. Div. of Mines and Geol., Sacramento, 1994.

Kennedy, B. M., Y. K. Kharaka, W. C. Evans, A. Ellwood, D. J. DePaolo, J. Thordsen, G. Ambats, and R. H. Mariner, Mantle fluids in the San Andreas fault system, California, *Science*, *278*, 1278–1280, 1997.

Kennedy, G. C., A portion of the system silica-water, *Econ. Geol.*, *45*, 629–653, 1950.

Kingery, W. D., H. K. Bowen, and D. R. Ulhmann, *Introduction to Ceramics*, 2nd ed., 1032 pp., John Wiley, New York, 1976.

Kirkwood, D., J. P. Gratier, A. M. Boullier, M. Ait Ougoudal, D. Marquer, Y. Géraud, M. Lespinasse, Connectivity and schistosity development in the Aar granodiorite, Switzerland: geometrical and chemical aspects of fluid-assisted deformation, Workshop on Fluids and Fractures in the Lithosphere, Univ. Nancy, Nancy, France, 1999.

Knopf, A., The Mother Lode system of California, *U.S. Geol. Survey. Prof. Pap.*, *157*, 88 pp., 1929.

Lachenbruch, A. H., Frictional heating, fluid pressure and the resistance to fault motion, *J. Geophys. Res.*, *85*, 6097–6112, 1980.

Lockner, D., and B. Evans, Densification of quartz powder and reduction of conductivity at 700°C, *J. Geophys. Res.*, *100*, 13,081–13,092, 1995.

Marquer, D., and M. Burkhard, Fluid circulation, progressive deformation and mass-transfert processes in the upper crust: The example of basement-cover relationships in the external crystalline massifs, Switzerland, *J. Struct. Geol.*, *14*, 1047–1057, 1992.

McCaig, A. M., and R. J. Knipe, Mass-transport mechanims in deforming rocks: Recognition using microstructural and microchemical criteria, *Geology*, *18*, 824–827, 1990.

Miller, S., A. Nur, and D. Olgaard, Earthquakes as a coupled shear stress-high pore pressure dynamical system, *Geophys. Res. Lett.*, *23*, 197–200, 1996.

Miller, S. A., Y. Ben-Zion, and J. P. Burg, A three-dimensional fluid-controlled earthquake model: Behavior and implications, *J. Geophys. Res.*, *104*, 10,621–10,638, 1999.

Molnar, P., Final report to the Southern California Earthquake Center for work performed during the period from September through December 1991, internal report, 126 pp., South. Calif. Earthquake Cent., Univ. of Calif., Los Angeles, 1993.

Oelkers, E. H., P. A. Bjørkum, and W. M. Murphy, A petrographic and computational investigation of quartz cementation and porosity reduction in North Sea sandstones, *Am. J. Sci.*, *296*, 420–452, 1996.

Paterson, M. S., Nonhydrostatic thermodynamics and its geologic applications, *Rev. Geophys.*, *11*, 355–389, 1973.
Petersen, M. D., and S. G. Wernousky, Fault slip rates and earthquake histories for active faults in southern California, *Bull. Seismol. Soc. Am.*, *84*, 1608–1649, 1994.
Pfiffner, O. A., and J. G. Ramsay, Constraints on geological rate: arguments from finite strain values of naturally deformed rocks, *J. Geophys. Res.*, *87*, 311–321, 1982.
Pili, E., B. M. Kennedy, M. S. Conrad, and J. P. Gratier, Isotope constraints on the involvement of fluids in the San Andreas fault, *Eos Trans. AGU*, *79*(17), S229–S230, Spring Meet. Suppl., 1998.
Pili, E., F. Poitrasson, and J. P. Gratier, Geochemical constraints on how fluids get into and out of faulted limestones from the San Andreas fault system: The role of host rocks in feeding dynamically organized fracture networks, *Chem. Geol.*, *190*, 229–248, 2002.
Poty, B., H. A. Stalder, and A. Weisbrod, Fluid inclusion studies in quartz from fissures of western and central Alps, Schweitz, *Mineral. Petrol.*, *54*, 717–752, 1974.
Raj, R., Creep in polycrystalline aggregates by matter transport through a liquid phase, *J. Geophys. Res.*, *87*, 4731–4739, 1982.
Raj, R., and C. K. Chyung, Solution-precipitation creep in glass ceramics, *Acta Metall.*, *29*, 159–166, 1981.
Ramsay, J. G., The crack-seal mechanism of rock deformation, *Nature*, *284*, 135–139, 1980.
Renard, F., P. Ortoleva, and J. P. Gratier, Pressure solution in sandstones: Influence of clays and dependence on temperature and stress, *Tectonophysics*, *280*, 257–266, 1997.
Renard, F., A. Park, P. Ortoleva, and J. P. Gratier, An integrated model for transitional pressure-solution in sandstones, *Tectonophysics*, *312*, 97–115, 1999.
Renard, F., J. P. Gratier, and B. Jamtveit, Kinetics of crack-sealing, intergranular pressure solution and compaction around active faults, *J. Struct. Geol.*, *22*, 1385–1407, 2000.
Rice, J. R., Fault stress states, pore pressure distributions, the weakness of the San Andreas fault, in *Fault Mechanics and Transport Properties in Rocks*, edited by B. Evans and T. F. Wong, pp. 475–503, Academic, San Diego, Calif., 1992.
Rice, J. R., and M. P. Cleary, Some basic stress diffusion solutions for fluid-saturated elastic porous media with compressible constituents, *Rev. Geophys.*, *14*, 227–241, 1976.
Robert, F., and W. C. Kelly, Ore-forming fluids in Archean gold-bearing quartz veins at the Sigma Mine, Abitibi greenstone belt, Quebec, Canada, *Econ. Geol.*, *82*, 1464–1482, 1987.
Robert, F., A. M. Boullier, and K. Firdaous, Gold-quartz veins in metamorphic terranes and their bearing on the role of fluids in faulting, *J. Geophys. Res.*, *100*, 12,861–12,879, 1995.
Rutter, E., The kinetics of rock deformation by pressure solution, *Philos. Trans. R. Soc. London, Ser. A*, *283*, 203–219, 1976.
Rutter, E. H., Pressure solution in nature, theory and experiment, *J. Geol. Soc. London*, *140*, 725–740, 1983.
Scholz, C., *The Mechanics of Earthquakes and Faulting*, 439 pp., Cambridge Univ. Press, New York, 1990.
Shimizu, I., Kinetics of pressure solution creep in quartz: Theoretical considerations, *Tectonophysics*, *245*, 121–134, 1995.
Sibson, R. H., Fault rocks and fault mechanisms, *J. Geol. Soc. London*, *133*, 191–213, 1977.
Sibson, R. H., Earthquake rupturing as a hydrothermal process, *Geology*, *15*, 701–704, 1987.
Sibson, R. H., Earthquake faulting, induced fluid-flow, fault-hosted gold-quartz mineralization, in *Characterization and Comparison of Ancient and Mesozoic Continental Margins—Proceedings of the 8th International Conference on Basement Tectonics (Butte, Montana, 1988)*, edited by M. J. Bartholomew et al., pp. 603–614, Kluwer Acad., Norwell, Mass., 1992a.
Sibson, R. H., Implications of fault-valve behavior for rupture nucleation and recurrence, *Tectonophysics*, *211*, 283–293, 1992b.
Sibson, R. H., F. Robert, and K. H. Poulsen, High angle reverse fault, fluid-pressure cycling and mesothermal gold quartz deposits, *Geology*, *16*, 551–555, 1988.
Sleep, N., and M. Blanpied, Creep, compaction and weak rheology of major faults, *Nature*, *359*, 687–692, 1992.
Smith, D. L., and B. Evans, Diffusional crack healing in quartz, *J. Geophys. Res.*, *89*, 4125–4135, 1984.
Spiers, C. J., and R. H. Brzesowsky, Densification behaviour of wet granular salt: Theory versus experiment, in *Seventh Symposium on Salt*, edited by H. Kakihana et al., pp. 83–91, Elsevier Sci., New York, 1993.
Tada, R., and R. Siever, Experimental knife-edge pressure solution of halite, *Geochim. Cosmochim. Acta*, *50*, 29–36, 1986.
Weir, R. H., and D. M. Kerrich, Mineralogy, fluid inclusion, stable isotope studies of several gold mines in the Mother Lode, Tuolumne and Mariposa counties, California, *Econ. Geol.*, *8*, 62–78, 1987.
Weyl, P. K., Pressure solution and the force of crystallization: A phenomenological theory, *J. Geophys. Res.*, *64*, 2001–2025, 1959.
Wilkins, R. W. I., J. P. Gratier, and L. Jenatton, Experimental observation of healing of cracks and the formation of secondary inclusions in halite and quartz, paper presented at European Current Research on Fluid Inclusions, Univ. Göttingen, Göttingen, Germany, 1985.
Wintsch, R. P., and J. Dunning, The effect of dislocation density on the aqueous solubility of quartz and some geologic implications: A theoretical approach, *J. Geophys. Res.*, *90*, 3649–3657, 1985.
Wintsch, R. P., R. Christoffersen, and A. K. Kronenberg, Fluid-rock reaction weakening of fault zones, *J. Geophys. Res.*, *100*, 13,021–13,032, 1995.
Yeats, R. S., G. F. Huftile, and L. T. Stitt, Late Cenozoic tectonics of the East Ventura basin, Transverse Ranges, California, *AAPG Bull.*, *78*, 1040–1074, 1994.
Zoback, M. D., Critically-stressed faults, deep crustal fluid flow and dynamic constraints on hydrocarbon migration, paper presented at Workshop on Fluids and Fractures in the Lithosphere, Univ. Nancy, Nancy, France, 1999.

P. Favreau, J.-P. Gratier, and F. Renard, LGIT, CNRS Observatoire, Université Joseph Fourier, Geosciences, BP 53X, F-38041 Grenoble cedex, France. (Jean-Pierre.Gratier@obs.ujf-grenoble.fr)